PD Dr. R. Schulze
Dept. of Oral Surgery (and Oral Radiology)
Johannes Gutenberg-University
Augustusplatz 2
55131 Mainz
Germany

Phone: ++496131173744
FAX: ++496131173434
rschulze@mail.uni-mainz.de

US Patent and Trademark Office
PO Box 1450,
Alexandria,
VA 22313-1450
USA

Mainz, 16/03/06

Dear Sirs,

I am contacting you with respect to a patent application, No: 10/813,499 entitled "Automatically conforming intraoral dental radiographic sensor". Fundamental parts of the features claimed in this applications are not novel, as you may see from two publications included with this mail. More specifically, besides a German Patent application in 2001 (which, of course is not relevant for the US) the correction of projective distortion using fiducial spherical reference bodies has been described in detail in an internationally published paper in 2002 [1]. We even extended the method for complete registration of projection geometry in another paper published in a high-standard (US-based) Journal in 2004 [2].
I believe, these papers should be considered in the patenting process for this particular application, particularly when novelty is targeted.
For your information, I enclose both papers together with the patent application with this mail.

Thank you very much for your kind attention to this objection. I would be very grateful, if you could send me some information on the final decision on that issue.

Sincerely,

Ralf Schulze

References:

1. Schulze, R., d'Hoedt, B., (2002). A method to calculate angular disparities between object and receptor in "paralleling technique". Dentomaxillofac Radiol; 31: 32-38.
2. Schulze, R., Brüllmann, D. D., Röder, F., d'Hoedt, B., (2004). Determination of projection geometry from quantitative assessment of the distortion of spherical references in single - view projection radiography. Med Phys; 31: 2849-2854.

US 20050226389A1

(19) United States

(12) Patent Application Publication (10) Pub. No.: US 2005/0226389 A1

Yoon et al. (43) Pub. Date: Oct. 13, 2005

(54) ANATOMICALLY CONFORMING INTRAORAL DENTAL RADIOGRAPHIC SENSOR

(75) Inventors: Douglas C. Yoon, Beverly Hills, CA (US); Adam Chen, Los Angeles, CA (US)

Correspondence Address:
Matthew F. Jodziewicz, Esq.
3447 Mandeville Canyon Road
Los Angeles, CA 90049-1019 (US)

(73) Assignee: Cyber Medical Imaging, Inc.

(21) Appl. No.: 10/813,499

(22) Filed: Mar. 31, 2004

Publication Classification

(51) Int. Cl.[7] H05G 1/64; G21K 4/00; A61B 6/14

(52) U.S. Cl. 378/191

(57) ABSTRACT

A system is described for obtaining intraoral radiographic images using an anatomically conforming sensor and a method is described for correcting the projective distortions caused by the inclination of the plane of the imaging sensor relative to the x-ray beam. The purpose of the described sensor system is to reduce patient discomfort as compared to conventional planar intra-oral x-ray sensors, which tend to impinge on sensitive tissues within the oral cavity. An additional purpose of the described system is to allow for better coverage of the subject by allowing the sensor to fit closer against the surrounding tissues.

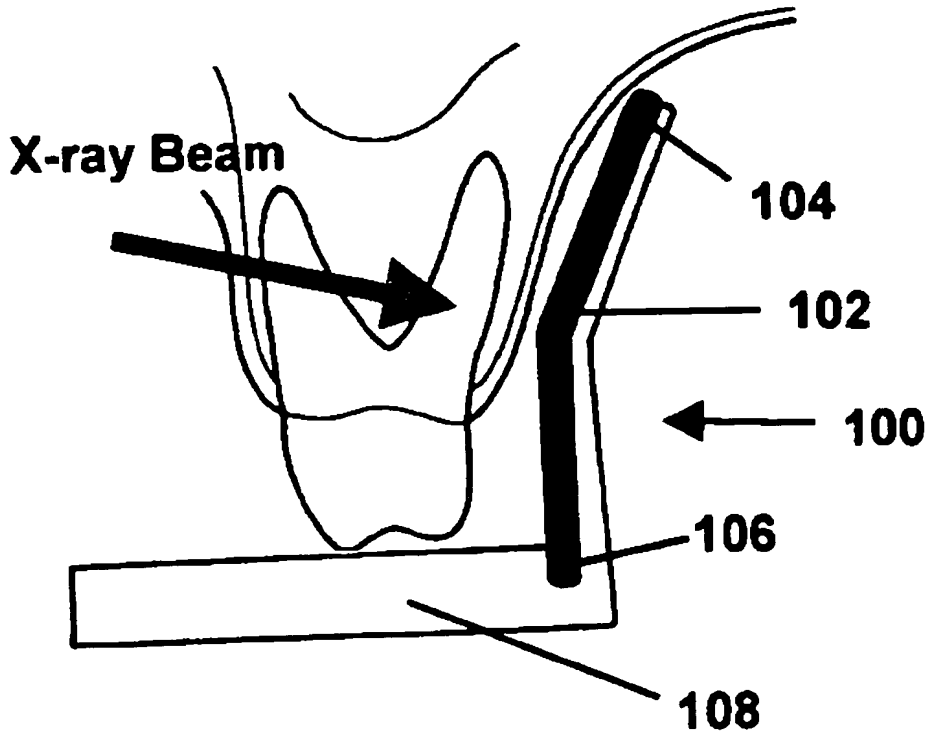

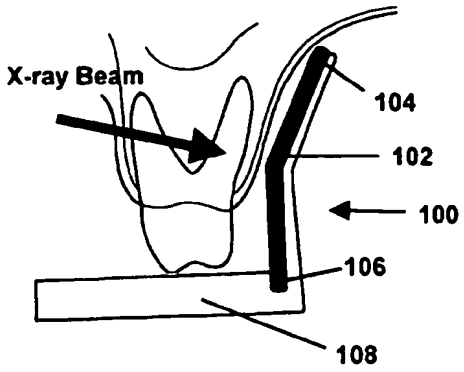

FIG. 1a

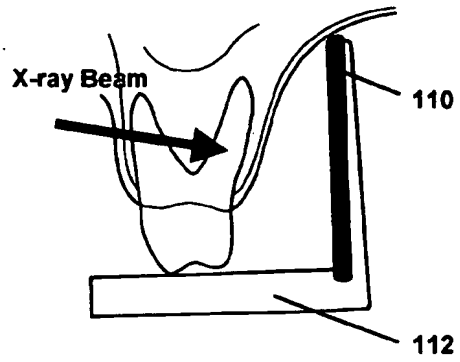

FIG. 1b

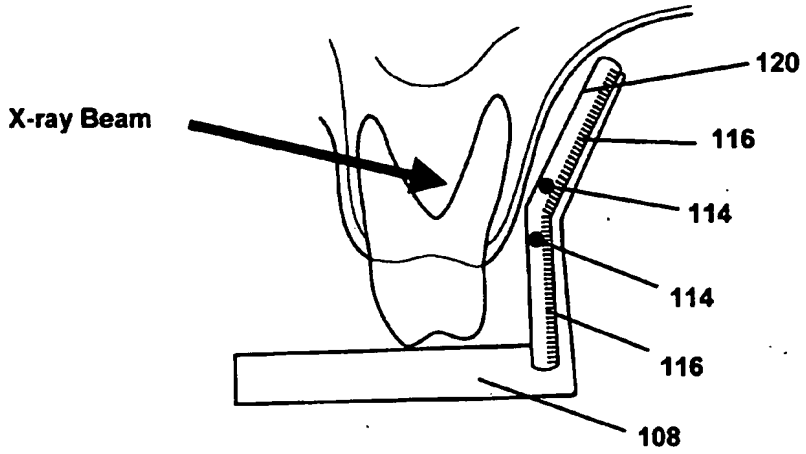
X-ray Beam
120
116
114
114
116
108

FIG. 2a

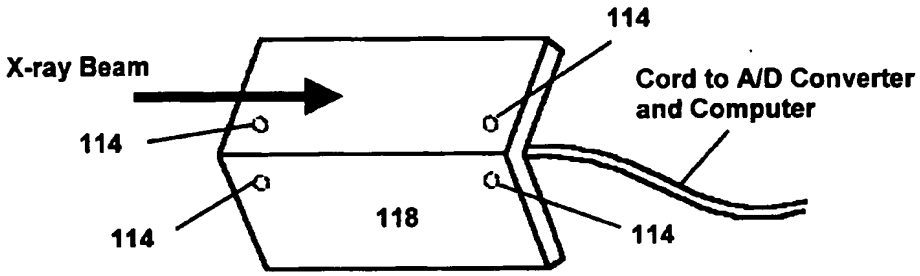
X-ray Beam
114
114
114
118
114
Cord to A/D Converter
and Computer

FIG. 2b

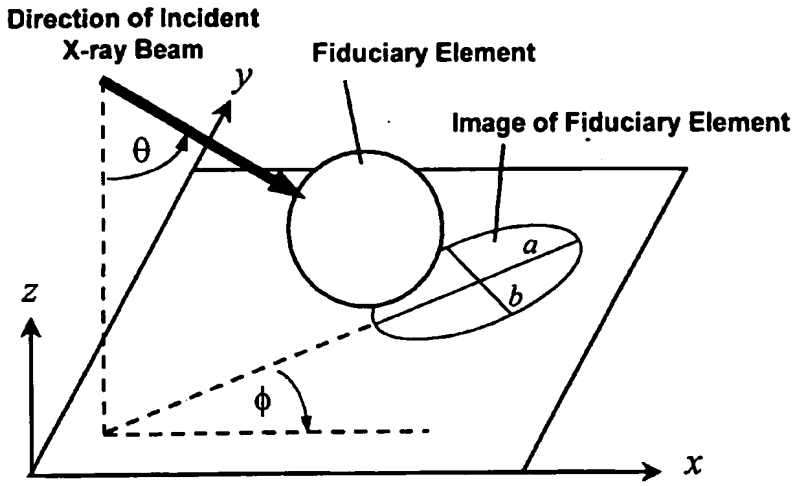
Direction of Incident
X-ray Beam
Fiduciary Element
Image of Fiduciary Element
y
θ
a
b
z
ϕ
x

FIG. 3a

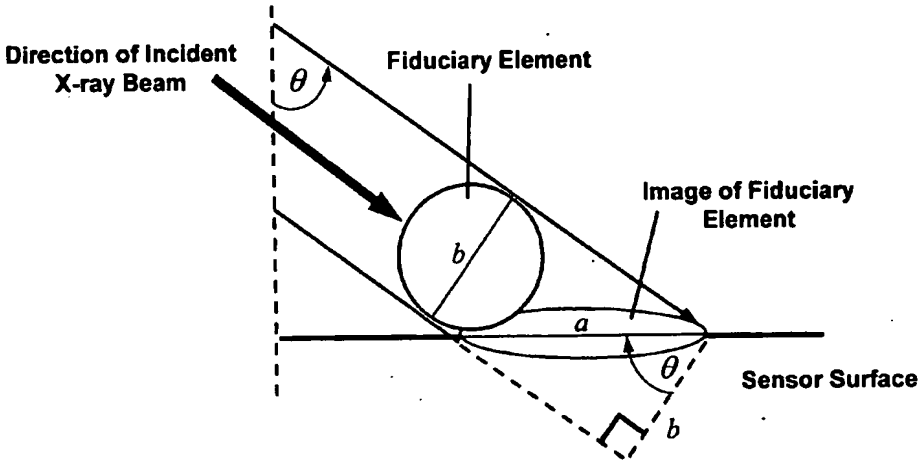
Direction of Incident
X-ray Beam
θ
Fiduciary Element
Image of Fiduciary
Element
b
a
θ
Sensor Surface
b

FIG. 3b

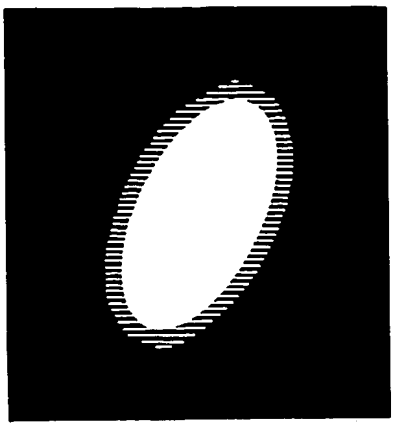

(a)

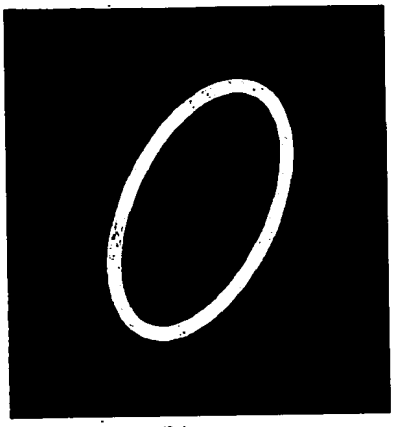

(b)

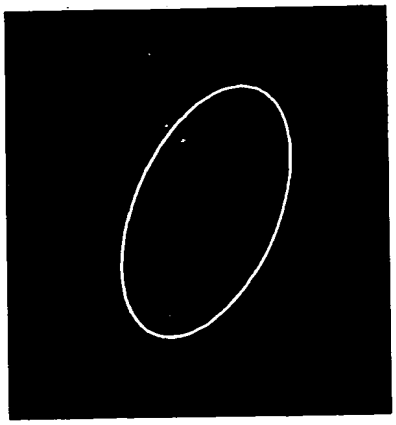

(c)

FIG. 4

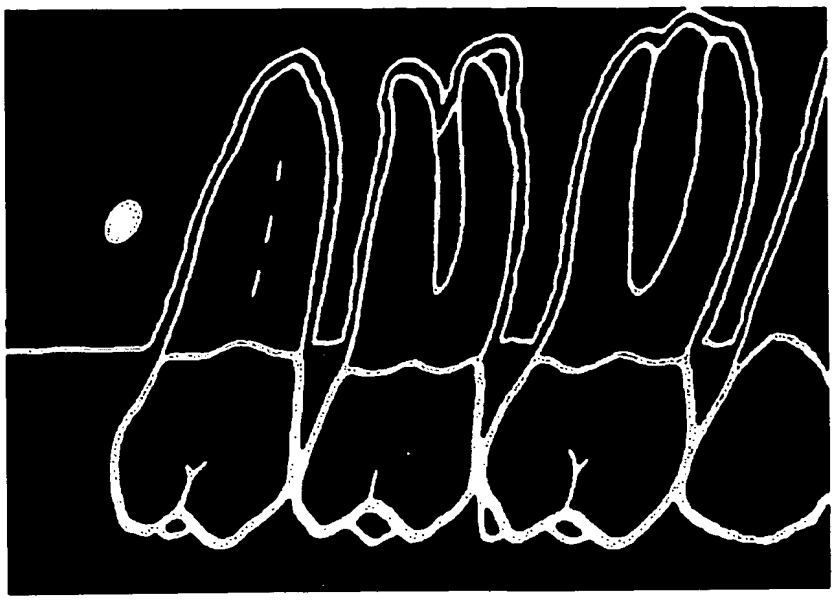

FIG. 5a

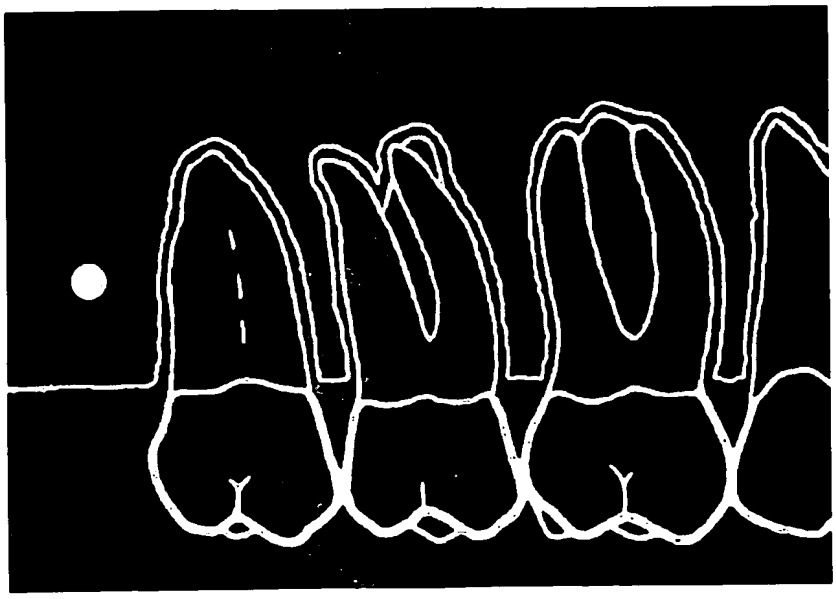

FIG. 5b

ANATOMICALLY CONFORMING INTRAORAL DENTAL RADIOGRAPHIC SENSOR

FIELD AND BACKGROUND OF THE INVENTION

[0001] The present invention relates to an intraoral sensor design to be applicable to radiographic imaging sensors such as film, storage phosphor devices or solid-state direct capture devices (e.g. CCD's or CMOS based devices) or any other imaging sensor that can be used to produce radiographic images. Such sensors may be components of radiographic imaging systems that may include computers and video monitors for displaying radiographs. The present invention is also directed toward a method of correcting distortions appearing in the images of such radiographic imaging systems caused by the non-perpendicularity of the x-ray source relative to the imaging surface. Such analyses may be performed on a PC, which in turn may be part of a digital radiographic imaging system. The illuminating x-ray radiation source for such sensors and radiographic imaging systems is not the subject of the present invention.

[0002] Radiographs are fundamental to most dental diagnostic procedures. However, a common complaint and problem during radiographic exams is patient discomfort during the placement of radiographic sensors within the mouth. The majority of these complaints involve the placement of the radiographic sensor in the posterior maxillary and mandibular arches of the patient. This problem is primarily due to the limited space available for proper placement of the sensors within these regions. This has been a problem since the inception of dental radiography using standard x-ray film technology.

[0003] A common method used to reduce such patient discomfort is to bend portions of the film package to conform to the anatomic shape of the mandibular or maxillary arches. However this bending contributes to the problems of image distortion of the intended subject as described below.

[0004] Recently, solid-state x-ray sensors have been developed that replace film. The patient discomfort problem for these sensors is even greater because these devices are rigid by nature and cannot be bent like film. With these rigid sensors, the only recourse is to place the sensor at a more comfortable angle and position for the patient, but such positioning is normally not optimal for a diagnostic radiograph of the intended subject. One study has shown that using such rigid devices results in more sensor placement errors than conventional film, thus requiring more retakes to produce clinically acceptable radiographs (C.H. Versteeg, et. al., *An evaluation of periapical radiology with a charge-coupled device*, Dentomaxillofacial Radiology, 1998, 27: 97-101).

[0005] Both of these approaches, using film and rigid sensors, result in a distorted radiographic image of the intended subject when the x-ray beam is not perpendicular to the imaging plane.

[0006] Thus, a need exists to provide for a more comfortable sensor configuration while correcting for the projective distortions of the images produced when the x-ray beam is not perpendicular to the imaging plane.

OBJECTS AND SUMMARY OF THE PRESENT INVENTION

[0007] Accordingly, an object of the present invention is to provide a configuration for a radiographic sensor that allows for increased patient comfort.

[0008] Another object of the present invention is to provide a configuration for a radiographic sensor that allows for improved coverage of the radiographic subject.

[0009] Yet another object of the present invention is to provide for the incorporation of fiduciary elements within a radiographic sensor that allows for the measurement of the magnitude of image distortion produced when the imaging x-ray beam is not perpendicular to the sensor surface.

[0010] Finally, another object of the present invention is to provide a method for the correction of distortions in a radiographic image that results when the x-ray beam is not perpendicular to the plane of the sensor.

[0011] The present invention is embodied in a radiation sensor that has a specific geometric shape or configuration that not only provides more comfort to a patient while in intraoral use, but one that is capable of providing a more accurate image of the area of concern by eliminating distortions of the resultant image normally found in other modern radiographic imaging systems and sensors. Such systems and sensors typically operate in conjunction with personal computer systems (PC's) whose function is to serve as a platform to receive, analyze, display and archive image data received from the sensor systems.

[0012] The preferred geometric configuration of a x-ray radiation imaging sensor that embodies the present invention is unique among known intraoral radiographic imaging sensors in that it divides the radiographic imaging sensor into several discrete sections, each section imaging a different region of the subject.

[0013] Furthermore such sections are arranged in a fashion that conforms to the anatomic curvatures of the human maxilla and mandible while maintaining a diagnostically useful image and contiguous coverage of the subject. To accomplish this the different sensor sections may be oriented in different directions, resulting in a non-planar shape.

[0014] Also, the sections of the sensor are abutted together in a fashion that yields contiguous coverage of the subject area. Finally, each section has incorporated within it radio-opaque fiduciary elements of known shape and size whose projected radiographic images indicate the orientation of the x-ray beam relative to the surface of each of the sensor sections.

[0015] Another embodiment of the present invention involves a method of processing of image data produced by the hardware that also embodies the present invention. This processing method includes steps that use the image of a fiduciary element, whose shape and size is known, to correct the projective distortions in the resultant radiographic image caused by non-perpendicularity of the x-ray beam relative to the surface of the sensor section.

[0016] Such inclination of the incident x-ray beam causes a projective distortion of the radiographic image of the fiduciary element, as well as the radiographic image of the intended subject. Because the shape and size of the fiduciary

element is known, the precise orientation of the x-ray beam can be derived from the nature of the distorted image using principles of projective geometry. In turn, the resultant distorted radiographic image can be restored to its undistorted state from knowledge of the beam orientation through a reverse projective transformation of the image, again using principles of projective geometry. This method of the invention is concerned with image distortion and restoration and is independent of the number of sensor sections and applies even to sensors consisting of only one section.

[0017] In general, one embodiment of the present invention is found in a radiation sensor that is intended for use with a digital intraoral radiographic imaging system for placement in the mouth of a patient for production of radiographs of teeth and supporting structures. Such a sensor includes a housing containing at least two generally planar, radiation detectors abutting at a non-zero angle forming a generally contiguous convex or concave image capturing surface oriented toward a radiation source. The housing shape is selected to conform to the anatomical curvatures of the human maxillary and mandibular arches of the average patient. At least one radio-opaque fiduciary element of known shape, size and location is embedded on, in or just under the housing intermediate to the radiation source and to the surface of each of the radiation detectors. The fiduciary elements cast a projected image on the surfaces of the radiation detectors when illuminated by an x-ray source for use in eliminating distortions in the image captured by the sensor.

[0018] Another embodiment of a sensor containing the present invention includes a radiation sensor also intended for use with a digital intraoral radiographic imaging system for placement in the mouth of a patient for production of radiographs of teeth and supporting structures that conforms to the anatomic oral structure of the patient in a manner that provides less distortion in the detected image than that of current sensors. In this embodiment the sensor is enclosed in a housing containing at least two generally planar, radiation detectors abutting at a non-zero angle to form a faceted, generally contiguous convex or concave image capturing surface oriented toward a radiation source. The angle is selected such that the sensor housing conforms to the anatomical curvatures of the human maxillary and mandibular arches of the average patient. In this embodiment, each adjoining pair of generally planar radiation detectors are held in a fixed angular relationship to one another or flexibly joined so that the angle at which they abut can be changed to allow the housing to conform more easily to the anatomical curvatures of the human maxillary and mandibular arches of the average patient.

[0019] Additionally, the present invention is also found in a method for correcting distortions in a radiation sensor used with a digital intraoral radiographic imaging system for placement in the mouth of a patient for the production of radiographs of teeth and supporting tissues. A method embodying the present invention includes the steps of:

[0020] Providing a housing containing at least two generally planar, radiation detectors abutting at a non-zero angle to form a faceted, generally contiguous convex or concave imaging surface oriented toward a radiation source, the angle being selected such that the sensor housing conforms more easily to the anatomical curvatures of the human maxillary and mandibular arches of the average patient;

[0021] Placing at least one radio-opaque fiduciary element of known shape, size and location intermediate to the radiation source and to the surface of at least one of the radiation detectors;

[0022] Exposing the surfaces of the radiation detectors and the fiduciary element to the radiation source to project an image of the fiduciary element and of the teeth and supporting structures onto the radiation detectors;

[0023] Capturing and digitizing for analysis the sensor output representing the projected image of the fiduciary elements and the teeth and supporting structures detected by the radiation detectors;

[0024] Analyzing the digitized data representing the image of the fiduciary element to determine the magnitude of distortion of the projected fiduciary element's shape onto the surfaces of the radiation detectors, due to the non-perpendicularity of the radiation source relative to the surfaces of the radiation detectors in comparison to that of an ideal undistorted image of the fiduciary element projected onto the surfaces of the radiation detectors by exposure to a radiation source that is perpendicular to the surfaces of the radiation detectors, and determining a corrective transformation that transforms the distorted image of the projected fiduciary element into that of an undistorted image of the fiduciary elements; and,

[0025] Applying the corrective transformation to the digitized image data to transform the distorted projected image of the teeth and supporting structures to that of an undistorted projected image of the teeth and supporting structures.

[0026] Various additional objects and advantages of the present invention will become apparent from the following detailed description.

BRIEF DESCRIPTION OF THE DRAWINGS

[0027] **FIG. 1*a*** is a cross-sectional view through the posterior portion of the maxilla illustrating an anatomically shaped radiographic sensor embodying the present invention;

[0028] **FIG. 1*b*** is a cross-sectional view through the posterior portion of the maxilla showing the placement of a conventional radiographic sensor and illustrating the potentially painful impingement of the sensor on the soft tissues of the palate;

[0029] **FIG. 2*a*** is a cross-sectional view through the posterior portion of the maxilla and an internal cross-sectional view of a section of an intraoral sensor illustrating an alternate anatomically shaped radiographic sensor with housing, radiation detectors and incorporated fiduciary elements embodying the present invention;

[0030] **FIG. 2*b*** is a frontal view of an alternate anatomically shaped radiographic sensor similar to that shown in **FIG. 2*a*** illustrating a possible spatial distribution of fiduciary elements within a sensor embodying the present invention;

[0031] **FIG. 3*a*** is an idealized schematic showing the projective geometrical relationship of a fiduciary element onto a plane;

[0032] **FIG. 3*b*** is a schematic showing the internal geometric arrangement of a fiduciary element with respect to the surface of the radiation detector in a section of a sensor and its projected image thereon;

[0033] FIG. 4*a* is an image of a spherical fiduciary element projected onto a sensor's radiation detector's surface;

[0034] FIG. 4*b* is an image of the spherical fiduciary element projected onto a sensor's radiation detector's surface as in FIG. 4*a* after the application of an edge filtering transformation to the image data;

[0035] FIG. 4*c* is the image of FIG. 4*a* after the image has been subjected to threshold and thinning filters;

[0036] FIG. 5*a* illustrates a distorted image of maxillary teeth due to excessive x-ray beam inclination; and,

[0037] FIG. 5*b* illustrates a corrected image of the distorted image of maxillary teeth as shown in FIG. 5*a* using the distortion of the projected images of the spherical fiduciary elements as a guide in correcting the distortion in the projected image plane.

DESCRIPTION OF THE PREFERRED EMBODIMENT OF THE INVENTION

[0038] Referring now to the Figures, a sensor embodying the present invention is shown generally at **100** in FIG. 1*a*. The simplest implementation of an anatomically shaped radiographic sensor **102** embodying the present invention has two abutted imaging planes **104, 106**, respectively, as shown in FIG. 1*a* which illustrates a cross-sectional view through the posterior portion of a patient's maxillary arch. A sensor holder/positioner **108** is shown for retention between a patient's teeth to hold sensor **102** in position during imaging procedures.

[0039] The specific angle of the two imaging planes **104, 106** relative to each other is not critical but empirical testing indicates that angles of about 20-40 degrees result in significant patient comfort relative to a single flat plane of equivalent imaging area. This configuration has been shown to significantly improve comfort and improve subject coverage compared to a standard sensor.

[0040] FIG. 1*b* is a similar view of a conventional radiographic sensor **110** and its corresponding sensor holder/positioner **112** illustrating the potentially painful impingement of the sensor on the soft tissue of the maxillary palate and the unfavorable imaging placement due to the increased distance of the sensor relative to the teeth and supporting structures.

[0041] FIG. 2*a* shows the placement of fiduciary elements **114** relative to the surfaces of the radiation detectors **116** of the sensor **102** and its housing **120**. Criteria for such elements include: 1) a size sufficiently small to minimize obstruction of critical features in the radiograph, 2) a size large enough to allow precise length measurement of the element relative to the resolution of the sensor, 3) radio-opacity of the element and, 4) as a manufacturing consideration the fiduciary element should be symmetrical in shape so that its precise orientation on the sensor is not critical.

[0042] FIG. 2*b* shows a frontal view of the preferred embodiment, illustrating the placement of the fiduciary elements **114** relative to the sensor surface **118**. Size and placement of such fiduciary elements **114** should strive to ensure imaging of at least one element per section of sensor, despite misaiming of the illuminating x-ray beam while minimizing obscuration of the intended subject.

[0043] Thus, in the preferred embodiment a 1 mm diameter stainless steel symmetric sphere has been selected as the fiduciary element **114** being illustrated. This is because stainless steel offers sufficient radio-opacity to the imaging X-ray beam, and also because currently available high-resolution CCD sensors typically have a pixel resolution of 0.022 millimeters (22 microns). Hence, the size measurement of the element should be accurate to about two percent (more than adequate for most dental diagnostic applications). Film offers even higher measurement accuracy.

[0044] The image distortions caused by non-perpendicularity of the illuminating x-ray beam relative to the surface of the radiation detector belong to a general class of mathematical functions known as projective transforms. Moreover, if the illuminating source is relatively far from the intended subject (far field approximation), a good approximation for dental imaging, then the distortion belong to a special sub-class of projective transforms known as affine transforms. In the case of the preferred embodiment such transforms result in a skewing or tilting of the image at angle ϕ and stretching of the image by a factor f, as given by the following general equation:

$$x' = x + y \cdot f \cdot \cos(\phi)$$

and

$$y' = y \cdot f \cdot \sin(\phi) \qquad \text{EQ. 1}$$

[0045] where (x, y) are the original image coordinates and (x', y') are the equivalent transformed or distorted image coordinates.

[0046] More importantly, if the values for the parameters ϕ and f can be determined then the image distortion effects can be corrected for by applying the reverse transformation of EQ. 1 as given by:

$$x = x' - \frac{y' \cdot \cos(\phi)}{\sin(\phi)} \text{ and } y = \frac{y'}{f \cdot \sin(\phi)} \qquad \text{EQ. 2}$$

[0047] where, (x, y) are the original image coordinates and (x', y') are the equivalent transformed or distorted image coordinates.

[0048] In turn, from geometric principles, the parameters ϕ and f are determined by the orientation of the illuminating x-ray beam relative to the surface of the radiation detector. Specifically, the skew angle, ϕ, is equal to the beam azimuthal angle and the stretch factor, f, in the far field depends upon the inclination angle, θ, of the beam relative to a perpendicular to the surface of the radiation detector by the relationship:

$$f_\theta = \frac{1}{\cos(\theta)} \qquad \text{EQ. 3}$$

[0049] However, it can be readily seen that the angle, ϕ and factor, f in EQ. 2 can be directly obtained from the extent and direction of elongation of the image of the spherical fiduciary element captured by the sensor, which is essentially the shadow of the fiduciary element cast upon the surface of the radiation detector by the illuminating x-ray beam.

[0050] FIGS. 3*a* and 3*b* are idealized schematics illustrating the geometric arrangement of a fiduciary element **114** with respect to the surface of the radiation detector **118** and the illuminating x-ray beam and the resulting image. Note that if the direction of the x-ray beam is perpendicular to the surface of the surface of the radiation detector, the image will be a circle. FIG. 3*b* shows the relationship between the beam inclination angle, θ, and the length of the major axis, a, under the far field assumption. The relationship defined in EQ. 3 can readily be deduced from FIG. 3*b*. Note that the length of the minor axis, b, is the same as the diameter of the fiduciary element.

[0051] From FIG. 3*a* it can be seen that if the beam is not perpendicular to the surface of the radiation detector then the shadow will be elongated and slanted or skewed at the same angle as the beam azimuthal angle, ϕ. Also, under the far field assumption, the shape will be an ellipse, where the length of the minor axis, b, will be the same as the diameter of the fiduciary element and the length of the major axis, a, will be longer than b by the factor, f, hence:

$$f = \frac{a}{b} \qquad \text{EQ. 4}$$

[0052] Even in the case of a non-planar parallel x-ray beam, more specifically, a divergent beam, the above derivation for f is robust. The beam divergence, here designated by Δθ, for most intraoral dental applications is typically less than 5 degrees. The error for f, defined as $f_{(\theta+\Delta\theta)}-f_{\theta}$ and denoted as Δf, can be calculated in terms of the beam divergence. More specifically, it can be shown from EQ. 3 that the fractional error for f, defined as Δf/f, is approximately:

$$\frac{\cos(\theta)}{\cos(\theta+\Delta\theta)} - 1 \qquad \text{EQ. 5}$$

[0053] For θ=0 degrees and Δθ=5 degrees the fractional error is less than 0.004 or 0.4 percent. For values of θas large as 30 degrees and Δ0=5 degrees the fractional error is less then 0.06 or 6 percent.

[0054] In addition, the error in the estimate of the skew or azimuth angle, ϕ, is not affected by beam divergence.

[0055] In practice, the parameters a, b and ϕ, for the elliptical images of the fiduciary elements ellipse can be extracted from the image data using image processing techniques and numerical methods. In the preferred embodiment this analysis is performed on a digital representation of the radiograph. Note that the actual image-capture technology for a digitized radiograph is not the subject of the present invention. Such images may be obtained indirectly by scanning conventional film radiographs with currently available digital film scanners or obtained directly using existing digital radiographic image capture technology such as storage phosphor plates or CCD/scintillator or CMOS/scintillator combinations.

[0056] The processing of image data in the preferred embodiment of the present invention is accomplished in two steps. First, the region of the digitized radiographic image that includes a fiduciary element is isolated based on its known position on the sensor. An example of such an image is shown in FIG. 5*a* for a spherical fiduciary element. Note the elliptical shape of the image due to the non-perpendicularity of the x-ray beam relative to the surface of the radiation detector capturing the image.

[0057] Next, the edges of the ellipse are emphasized using gradient filtering (e.g. Sobel filter) as illustrated in FIG. 5*b*. An intensity threshold is applied to the filtered image to extract image points in the edge region of the ellipse, and then these points are thinned or eroded using standard numerical techniques in order to more precisely define the edge region. These extracted points are shown in FIG. 5*c*. These points are used in the derivation of the curve fitting parameters. To this end, the set of extracted edge points (white points) in FIG. 5*c* are tabulated in terms of their pixel coordinates (i.e. x and y pixel coordinates).

[0058] The coordinates of the tabulated points are applied to the fitting of an equation for a generalized ellipse oriented at angle, ϕ, with major axis length, a, and minor axis length, b, and centered about (x_0, y_0) as given by:

$$\frac{\left[(x-x_0)\cdot\cos(\phi)-(y-y_0)\cdot\sin(\phi)\right]^2}{a^2}+\frac{\left[(x-x_0)\cdot\sin(\phi)+(y-y_0)\cdot\cos(\phi)\right]^2}{b^2}=1 \qquad \text{EQ. 6}$$

[0059] Note that EQ. 6 is not the same as the image distortion transformation due to beam non-perpendicularity, but rather just the equation of a rotated ellipse used to estimate, the orientation parameters of interest, ϕ, a, b.

[0060] The best estimate for the unknown parameters, ϕ, a, b, x_0, and y_0 are derived through least squares error minimization, minimizing the summed squared error between the coordinates of the tabulated extracted feature points and their corresponding equivalent points on the parameterized ellipse given by EQ. 6. In the preferred embodiment, an initial estimate is made for the unknown parameters based on an undistorted image and corresponding pairs of points are found by taking the nearest point on the parameterized ellipse to each extracted feature point. This approach, when applied iteratively, rapidly converges to an error minimum. In general, all such methods of initial parameter approximation and method of pairing corresponding points is claimed.

[0061] Once the best estimate for the unknown parameters, ϕ, a, b, x_0, and y_0 are derived one can then use the estimate of the parameters a and b to calculate the factor f through EQ. 4

[0062] Note that in this specific example, the expression is not linear in all the parameters, ϕ, a, b, x_0, and y_0, thus linear least squares fitting methods do not apply. However, numerous non-linear methods exist, such as iterative application of gradient descent error minimization. Also note, the use of other shapes for fiduciary elements, in other embodiments of the present invention may be chosen that offer more direct solutions to the orientation parameters. Finally, other methods besides least squares error minimization may be applied to derive estimates of the beam orientation parameters. The

present invention is intended to cover all such fiduciary element configurations and methods of deriving orientation parameters from the image of such elements.

[0063] The final step is to apply the corrective transformation in EQ. 2 to the digitized image based on the derived values ϕ and f.

[0064] As an example of the effectiveness of the technique, **FIG. 5*a*** shows an example of a radiographic image from a bi-planar sensor with imbedded 1 mm spherical fiduciary elements. Note the distortion, specifically elongation, of the roots of each maxillary tooth and the corresponding elongation of the fiduciary elements due to excessive x-ray beam inclination.

[0065] **FIG. 5*b*** shows the result of correction of the image in **FIG. 5*a*** using the extent of elongation of the fiduciary elements to correct the image. Note with the corrected image the fiduciary elements are restored to a circular shape.

[0066] In view of the above, it will be seen that the several objects of the invention are achieved and other advantageous results attained.

[0067] As various changes could be made in the above construction and methods without departing from the scope of the invention, it is intended that all matter contained in the above description or shown in the accompanying drawings shall be interpreted as illustrative and not in a limiting sense.

We claim:

1. A radiation sensor for use with a digital radiography imaging system for intraoral placement in a mouth of a patient for production of radiographs of teeth and supporting structures, said sensor comprising:

a housing containing at least one generally planar, radiation detector providing an imaging surface oriented toward a radiation source, said housing conforming to the anatomic curvatures of the human maxillary and mandibular arches of the average patient; and,

at least one radio-opaque fiduciary element of known shape, size and location positioned intermediate the radiation source and the surface of said at least one radiation detector, said at least one fiduciary element casting a projected image on said at least one radiation detector when illuminated by a radiation source.

2. A radiation sensor as in claim 1 wherein said housing contains at least two, generally planar, radiation detectors abutting at a non-zero angle to form a faceted, generally contiguous imaging surface oriented toward the radiation source, said angle selected to conform said housing to the anatomic curvatures of the human maxillary and mandibular arches of the average patient.

3. A radiation sensor as in claim 2 wherein each adjoining pair of said generally planar detectors abut one another at a fixed angle.

4. A radiation sensor as in claim 2 wherein each pair of adjoining generally planar radiation detectors are flexibly joined so that the angle at which they abut can be changed to conform said housing to the anatomic curvatures of the human maxillary and mandibular arches of the average patient.

5. A radiation sensor as in claim 2 wherein said fiduciary element is a sphere.

6. A radiation sensor as in claim 1 wherein said fiduciary element has a shape whose projected image on the surfaces of said radiation detectors includes at least two intersecting line segments.

7. A radiation sensor as in claim 1 further comprising at least one radio-opaque fiduciary element of known shape, size and location embedded on, in or under said housing intermediate the radiation source and the surface of each of said at least one radiation detectors, said at least one fiduciary element casting a projected image on said at least one radiation detectors when illuminated by an x-ray source.

8. A radiation sensor as in claim 1 wherein said housing further having a holding tab protruding therefrom for retention between the teeth for holding the radiation detectors in a fixed position in the patient's mouth.

9. A radiation sensor for use with a digital radiography imaging system for intraoral placement in a mouth of a patient for production of radiographs of teeth and supporting structures, said sensor comprising:

a housing containing at least two, generally planar, radiation detectors abutting at a non-zero angle to form a faceted, generally contiguous imaging surface oriented toward the radiation source, said angle selected to conform said housing to the anatomic curvatures of the human maxillary and mandibular arches of the average patient, said teeth and supporting structures casting a projected image on said at least two radiation detectors when illuminated by a radiation source.

10. A radiation sensor as in claim 9 wherein each adjoining pair of said generally planar detectors abut one another at a fixed angle.

11. A radiation sensor as in claim 9 wherein each pair of adjoining generally planar radiation detectors are flexibly joined so that the angle at which they abut can be changed to conform said housing to the anatomic curvatures of the human maxillary and mandibular arches of the average patient.

12. A radiation sensor as in claim 9 wherein said housing further having a holding tab protruding therefrom for retention between the teeth for holding the radiation detectors in a fixed position in the patient's mouth.

13. A method for correcting distortions in a radiation sensor used with a digital radiography imaging system for intraoral placement in a mouth of a patient for production of radiographs of teeth and supporting structures, said method comprising the steps of:

Providing a housing containing at least one generally planar, radiation detector providing an imaging surface oriented toward a radiation source, said housing conforming to the anatomic curvatures of the human maxillary and mandibular arches of the average patient;

Placing at least one radio-opaque fiduciary element of known shape, size and location positioned intermediate a radiation source and the surface of said at least one radiation detector, said at least one fiduciary element casting a projected image on said at least one radiation detector when illuminated by the radiation source.

Exposing said at least one radiation detector and said at least one fiduciary element to the radiation source to project an image of said at least one fiduciary element and said teeth and supporting structures onto the surface of said at least one radiation detector;

Capturing and digitizing the data representing the projected image of the fiduciary element, teeth and supporting structures images on the surface of said at least one radiation detector produced by the radiation detector;

Analyzing the digitized image data to determine the distortion of the projected fiduciary shape onto the surface of the at least one radiation detectors due to the non-perpendicularity of the radiation source with respect to the surface of the at least one radiation detectors from that of a ideal fiduciary image projected onto the surfaces of the at least one radiation detectors by exposure to a radiation source perpendicular to the surface of the at least one radiation detectors, and determining a corrective transformation that transforms the distorted projected fiduciary shape to that of the ideal fiduciary shape; and,

Applying the corrective transformation to the remaining digitized image data in order to transform the distorted projected image of the teeth and supporting structures to that of an ideal projected image of the teeth and supporting structures.

14. A method as in claim 13 further including the step of:

Placing a radio-opaque fiduciary element of known shape, size and location intermediate the radiation source and the surface of each one of said at least one radiation detector.

15. A method as in claim 14 wherein the step of placing at least one radio-opaque fiduciary element of known shape, size and location intermediate the radiation source and the surface of each one of said at least one radiation detectors, further includes the step of:

Embedding on, or placing in or under said housing at least one radio-opaque fiduciary element of known shape, size and location intermediate the radiation source and the surfaces of each of said at least one radiation detectors, said at least one fiduciary element casting a projected image on the surfaces of said at least one radiation detectors.

* * * * *

#1

Dentomaxillofacial Radiology (2002) 31, 32–38

www.nature.com/dmfr

A method to calculate angular disparities between object and receptor in 'paralleling technique'

RKW Schulze*,[1] and B d'Hoedt[1]

[1]*Department of Oral Surgery, Dental School, Johannes Gutenberg University, Mainz, Germany*

Objective: To develop an image analysis method for calculation of angular disparities between an object, temporarily equipped with a reference system, and a radiographic receptor.
Materials and methods: A mathematical method based on a reference system containing two metallic spheres is developed, allowing calculation of inclination between the inter-spherical axis and the digital image receptor using image features. Experimental evaluation was done in standardized projection geometry for two sphere sizes at four randomly chosen inclinations per size, with each radiograph assessed three times. Truth was assessed threefold from photographs obtained at each inclination.
Results: Mean standard deviation between single assessments was 2.6°. Significant differences (P Maloney/Rastogy = 0.00) were found between absolute values of truth and calculated values (mean: −0.9°; range: −6.0°; 3.6°), indicating a significant lack of accuracy.
Conclusions: Although so far not sufficiently accurate, the method yields information relevant for correction of distortion in intra-oral radiology.
Dentomaxillofacial Radiology (2002) **31**, 32–38. DOI: 10.1038/sj/dmfr/4600657

Keywords: image processing, computer-assisted; computer simulation; radiography, dental

Introduction

Geometric discrepancy between serial X-rays may indicate differences that do not reflect anatomical changes.[1] Standardization of the imaging geometry is therefore a prerequisite of utmost importance, if accurate measurement of such changes is required. According to a fundamental study of van Aken the most desirable projection is obtained, when (1) parallel rays are used due to infinite distance between focal spot and object, and (2) the X-rays meet both film and object at right angles.[2] Since criterion (1) cannot be achieved as the focus is always at a finite distance to the object, the paralleling technique was introduced in dental radiology as a good compromise. While a rigid holding device provides a perpendicular alignment of the central ray relative to the receptor, true parallelism between receptor and object is hardly feasible in a clinical environment, particularly in the upper jaw. Often the object and receptor plane are not parallel, resulting in a non-affine and irreversible distortion of the image as a function of degree of actual inclination.[3,4] Angular differences between two exposures can be derived mathematically from images, if radiographically detectable landmarks of known dimensions are present and the geometric relation between focus and object is fixed.[5–7] However, no method exists to calculate the actual angulation of the receptor plane relative to the object in one radiographic image. In tuned aperture computed tomography (TACT) metallic spheres can be used as fiducial markers to obtain the center of gravity for reconstruction of the TACT image.[8] In addition, six or less spherical references can be used to determine the geometrical positions of the X-ray source, if the object is equipped with references and a back projection algorithm used.[9] In contrast to this method, our approach is aiming to determine angular disparities in paralleling X-ray projection by quantitative analysis of the elliptical shape of two spherical references and by location of their shadows.

We based our investigation on the fact that magnification is always directly proportional to the distance of an object from the projection plane.[10]

*Correspondence to: R Schulze, Poliklinik für Zahnärztliche Chirurgie, Augustusplatz 2, 55131 Mainz, Germany. E-mail: rschulze@mail.uni-mainz.de
Received 2 June 2001; revised 29 August 2001; accepted 9 September 2001

Hence, by means of a reference object of known dimensions, the position of the object within an otherwise fixed projection system can be derived from its magnification. We believe that the angular relationship of object to receptor may be obtained from quantitative image analysis using two reference spheres temporarily attached to an object with their main axis aligned with the object.

The aim of this investigation was to calculate the angular disparity of an object relative to the receptor, based on the application of reference objects and a perpendicular orientation of the central X-ray to the image receptor.

Materials and methods

Mathematical theory

The following method is restricted only to the paralleling technique and is based on the fact that transmission radiography of an object with rotational symmetry, such as a sphere, will only be distorted in one direction, depending on its actual position in the projection system. If the central ray passes through the center of the sphere the resulting image will be a disc, but deviation from this path will produce an elliptical image of the sphere. The magnitude of the distortion is a function of three factors: (1) the distance between the focal spot and the sphere as measured along the central ray ($\overline{FX_v}$); (2) the distance between the sphere and receptor as measured along the central ray ($\overline{X_vO'}$); and (3) the shortest distance of the sphere from the central ray of the beam (d) (Figure 1). If the dimensions of the sphere and the focus to receptor distance ($\overline{FO'}$) are known, its actual position in a 3-D coordinate system with the x-axis aligned to the central ray can therefore be derived directly from the image. When a second sphere is applied, the inter-sphere axis ($\overline{M_1M_2}$) as defined by the line connecting both centers determines the actual inclination relative to a receptor axis of interest.

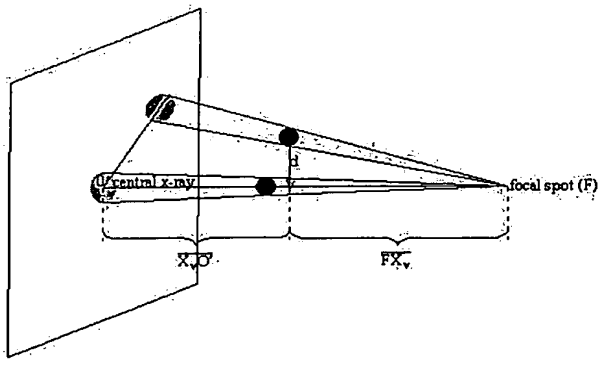

Figure 1 Underlying projection geometry resulting in one-dimensional distortion of objects with rotational symmetry (spheres) in transmission radiography. Note the elliptical distortion caused if the central X-ray is not passing through the center of the sphere. $\overline{X_vO'}$ = object to receptor distance; $\overline{FX_v}$ = focus to object distance; d = shortest distance between center of sphere and central X-ray

Our calculations are based on the following assumptions:

(1) the focal spot (F: X_F, 0, 0) is approximated by a point, located on the x-axis of the 3-D coordinate system (X, Y, Z) with the central ray aligned with the x-axis meeting the receptor surface at point zero (O': 0; 0; 0),
(2) X-rays are described by linear rays,
(3) y- and z-axes define the horizontal and vertical longitudinal axes of the flat receptor,
(4) the inclination is calculated in relation to an axis of interest of the receptor (here: vertical axis (z)), with $\overline{M_1M_2}$ being orientated relatively parallel to this axis in the $y-z$-plane.
(5) the position of the central ray on the receptor surface and the focus to receptor distance ($\overline{FO'}$) are known.
(6) the position of the focal spot is not colinear with the centers of the reference spheres.

All subjects of interest are graphically illustrated in Figure 2. For simplification reasons, the following explanations are presented in a generalized manner with the index i replacing the number of the sphere (1, 2). The upper sphere is referred to as sphere No. 1, the lower sphere as sphere No. 2. Let the objects located in the image plane be indicated by a superscript dot-dash ('). The centers of the spheres are denoted by M_i, their images as M'_i, respectively. R'_i and S'_i represent the outer and inner intersections of the image ellipse with the line passing through O' and M_i' ($\overline{O'M'_i}$). The angle α_i is the outer angle defined by R'_i, F and S'_i, the inner angle β_i by S'_i, F and O'. We obtain the angles α_i and β_i from:

$$\alpha_i = \frac{\overline{R'_iO'}}{\overline{O'F}} - \beta_i = \arctan\frac{\overline{R'_iO'}}{\overline{O'F}} - \arctan\frac{\overline{S'_iO'}}{\overline{O'F}} \quad (1)$$

We now need to calculate the distance $\overline{M_iF}$ of the center of the sphere (M_i) from the focal spot F. By introduction of an auxiliary plane defined by $O'M'_i$ and F we can calculate $\overline{M_iF}$ as follows:

$$\overline{M_iF} = \frac{r_i}{\sin\left(\frac{\alpha_i}{2}\right)} \quad (2)$$

where r_i is the radius of the sphere i. Since we are interested in the distance of Mi_i relative to the vertical axis (z) of the receptor, we have to find the projection V_i (X_{vi}, Z_{vi}) of M_i onto a plane defined by x- and z-axis of the coordinate system. To obtain these coordinates, we first have to construct the image of V_i (V'_i) by drawing a perpendicular line to the vertical axis z through M'_i. We then need to calculate the angle ε between the X-ray passing through M_i and $\overline{M_iX_{v_i}}$ in terms of:

$$\varepsilon = 90° - \beta_i - \frac{\alpha_i}{2} \quad (3)$$

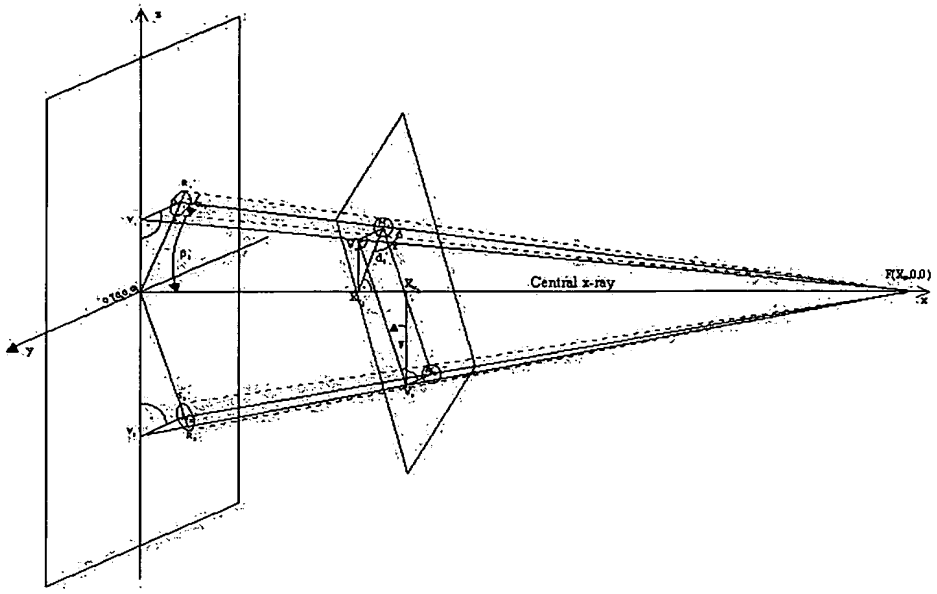

Figure 2 Geometrical construction for mathematical approach. The point of incidence of the central X-ray on the receptor (point zero: O'(0,0,0)) has to be known. R and S denote the outer and inner interception between the ellipse of the sphere image and the line through O' and the center of the elliptical image of each sphere. Detailed description of all other distances and landmarks is given in the text

X_{Vi} is derived from:

$$X_{V_i} = \overline{FO'} - \overline{FX}_{V_i} \tag{4}$$

with:

$$\overline{FX_{V_i}} = \overline{M_iF}\sin\varepsilon \tag{5}$$

To clarify the underlying mathematics of the following steps a plane projection extracted from Figure 2 is presented in Figure 3. Z_{Vi} is obtained from the normal equation (eq.) of linear functions in terms of:

$$Z_{V_i} = -X_{V_i}\frac{\overline{V'_iO'}}{\overline{FO'}} + \overline{V'_iO'} \tag{6}$$

Please note, that the vertical position of V'_1 and V'_2 to point zero (O') is essential for further calculations, since it determines the direction of inclination. $\overline{V'_iO'}$ is signed positive, if V' is located above and, vice versa, $\overline{V'_iO'}$ is signed negative, if V' is located below point zero. Since we now have defined the X and Z coordinates (X_{Vi}, Z_{Vi}) of the projection of each spheres' actual position in the projection system onto the vertical receptor plane, we can now calculate the actual inclination γ of $\overline{M_1M_2}$ relative to the vertical axis of the receptor from:

$$\gamma = \arctan\frac{X_{V1} - X_{V2}}{Z_{V1} - Z_{V2}} \tag{7}$$

with γ signed positive, if $X_{V1} \geq X_{V2}$, meaning that $\overline{M_1M_2}$ is inclined with its upper part towards the focal plane. Vice versa γ will be signed negative, if

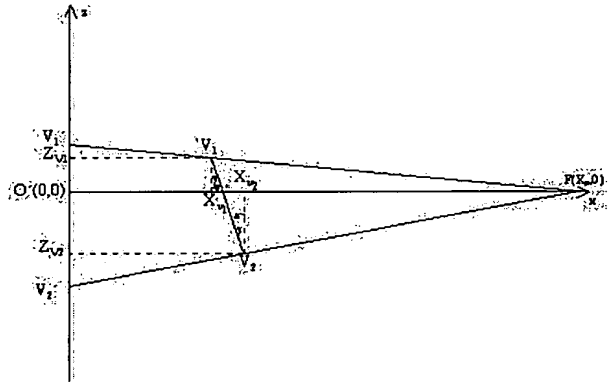

Figure 3 Two-dimensional projection extracted from Figure 2 for clarification of equations (6) and (7), which are necessary to obtain the actual angulation relative to the receptor. $V_1(X_{V1}; Z_{V1})/V_2$ (X_{V2}; Z_{V2}) represent the projection of the centers of the reference spheres (M_1/M_2) on the vertical plane defined by focal spot (F) and vertical receptor axis. For further descriptions see Figures 1 and 2

$X_{V1} < X_{V2}$, indicating an angulation of $\overline{M_1M_2}$ with its top towards the receptor plane.

Experimental set-up

Experimental evaluation of the mathematical algorithm was performed by means of a projection system fulfilling the criteria as described above (Figure 4). Two steel balls (diameter: 3.15 mm) were embedded

13 mm apart from each other in clear autopolymerizing resin in a small clear acrylic tube (length = 30 mm; diameter = 9.0 mm), with a minimum of 5 mm resin covering the balls on both sides. The same procedure was carried out with two additional steel balls of 5.00 mm diameter. Both tubes were then cut at one end in such a way, that an oblique bevel resulted which was then glued to the top of a screw (M8; length = 20 mm). A three-sided open box (length = 14 cm; width = 12 cm; height = 12 cm) made of wood was constructed with walls standing perpendicularly to each other. In the following the long vertical wall (14 cm) will be referred to as back wall, and the smaller (12 cm) vertical wall as front wall. On the ground surface of the box a plastic positioning ring of a commercially available film holding device (RWT, model anterior, Kentzler-Kaschner Dental GmbH, Germany) was fixed with the ring being in parallel position to the front wall at a distance of 48.0 mm. This positioning ring has a flat front side and a back side with a rectangular notch exactly fitting to the end-piece of the radiographic tube (Heliodent MD, Sirona Dental Systems GmbH, Bensheim, Germany). A disc of exactly the size of the outer diameter of the positioning ring (74.0 mm) made of thin (0.1 mm) clear plastic foil and containing a small metal ball (marking sphere; diameter = 0.80 mm) fixed in its center was concentrically glued to the front side of the ring. At a distance of 21.0 mm from the front wall the corresponding nut of the screw was mounted on the ground surface in such a way, that it was positioned slightly laterally to the central X-ray when the tube was connected to the positioning ring. By turning the screw in the corresponding nut various inclinations of the two-ball-system relative to the receptor could be produced. To obtain information on the actual inclination of the reference device relative to the vertical axis of the receptor, millimeter-scaled paper was glued on to the back wall of the box aligned with the vertical axis of the front wall. A CCD-image receptor ($40 \times 24 \times 6$ mm) providing high resolution (Trophy RVG 5, Trophy Radiologie S.A., Marne la Valle, France) was rigidly mounted on to the front wall with its active surface in beam direction and the vertical (= long) edge aligned parallel to the back wall of the box. Containing an active array of 30×20 mm this sensor yields a resolution of 1 572 864 pixels with each pixel being 19.5×19.5 μm^2. One option included in the proprietary software of the manufacturer (Trophy Windows Version 4.1k) is 1 : 1 pixel-binning, meaning that one sensor pixel will be represented by one image pixel. The sensor was interfaced to a personal computer (Intel Pentium III-MMX). After rigid fixation of the tube in the corresponding notches of the positioning ring by means of adhesive tape a series of four radiographs with each tube positioned in its nut was taken (60 kVp, 7 mA, 0.10 s) with different randomly chosen inclinations of the two-sphere system. For each inclination a photograph was obtained with a digital camera (FinePix S1 Pro, Fuji Photo Film (Europe) GmbH, Düsseldorf, Germany) positioned approximately 1 m distant to the box so that its optical axis was aligned with a theoretical line parallel to the front wall of the box through the center of the screw. Due to this set-up minimal distortion of the photos (jpeg-files) was guaranteed. Radiograph (tiff-file) and corresponding photography (jpeg-file) were exported and each pair was encoded for subsequent image evaluation. All relevant projection parameters are listed in Table 1.

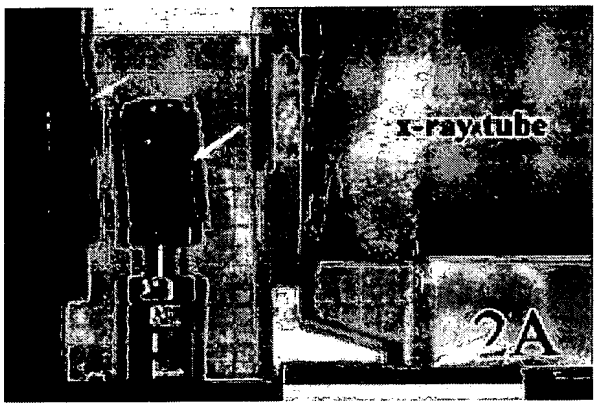

Figure 4 Photo of experimental set-up of the situation encoded as image 2A. The left arrow is indicating the CCD-sensor, the right arrow the tube containing the two reference spheres presenting a forward (negative) angulation relative to the CCD-receptor. Light refraction of the clear resin within the cylindrical tube functioning as convex lens causes horizontal widening of the spheres in the photography. All relevant distances and dimensions are listed in Table 1

Table 1 Projection and exposure parameters for the experimental evaluation

Focus to receptor distance ($\overline{FO'}$)	261.15 mm
Distance between marking sphere and receptor	45.30 mm
Diameter of the two reference spheres (r_1, r_2)	r_1: 5.00 mm, 4 exposures r_2: 3.15 mm, 4 exposures
Distance between reference spheres	r_1:13.35 mm r_2:16.35 mm
Pixel size of receptor RVG5	0.0195 mm^2
Exposure parameters	60 kVp, 7 mA, 0.10 s

Image evaluation

Radiographs were examined by image-editing software (Adobe Photoshop 5.0, Adobe Software Inc. Mountain View, CA, USA) and then evaluated on a 1 : 1 display monitor (1028 × 728 pixels) with each image pixel represented by one monitor pixel (Figure 5). The actual length of an image path can be calculated from the number of pixels and their length (19.5 μm) by the Pythagorean theorem. After brightness and contrast enhancement of the radiograph, the center of the circular image of the marking sphere (O′: 0; 0; 0) was constructed by bisecting the horizontal and vertical maximum diameter. Subsequently, tangents to both sides of the images of each reference sphere were drawn and the resulting distance between the tangent points at each sphere bisected. By connecting O′ to this bisecting point we obtain the axis along which the sphere is distorted, and consequently, the construction points R_i' and S_i'. By again bisecting the distance between R_i' and S_i' we obtain point M_i'. The intersection between a line through point O′ parallel to the long image axis and a perpendicular dropped to this line through M_i' defines V_i' (Figure 5). Now the distances required for the calculation ($\overline{R_1'O'}$, $\overline{R_2'O'}$, $\overline{S_1'O'}$, $\overline{S_2'O'}$, $\overline{V_1'O'}$, $\overline{V_2'O'}$) were measured to the nearest pixel and the values transferred in a spreadsheet software (Microsoft Excel 2000), where the resulting lengths were calculated. Again these values were transferred into another spreadsheet incorporating the described algorithm, and γ was calculated for each radiograph. The whole construction and measurement procedure was repeated threefold by one examiner (RS), with the mean value representing 'calculated inclination'.

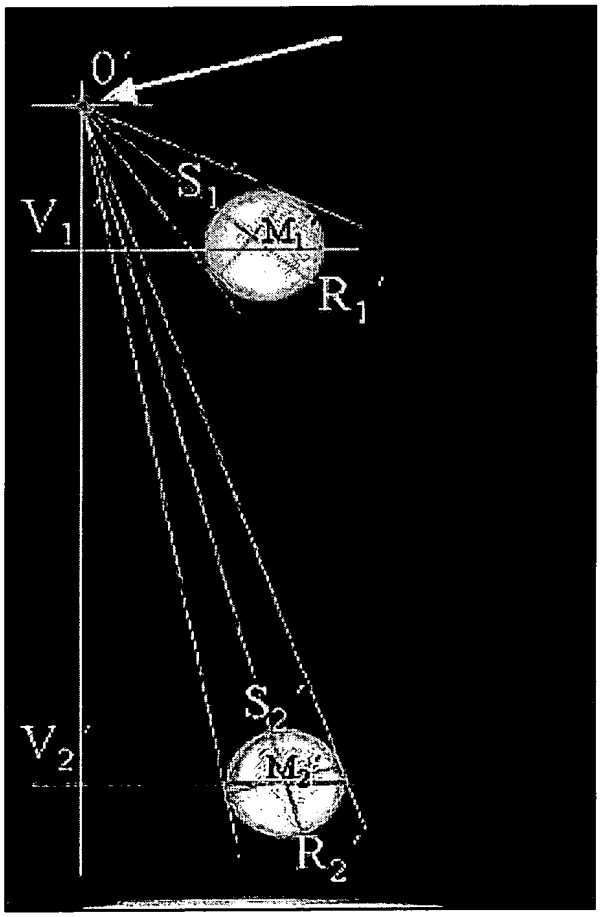

Figure 5 Geometrical construction on a radiographic image obtained with the experimental set-up, required to extract all relevant information on distortion for calculation of actual angulation. For better understanding landmark points as introduced in Figure 2 are included in the image. The arrow is indicating the circular image of marking sphere, with its center representing the point of incidence of central X-ray (point zero: O′ (0; 0; 0))

The corresponding photographs were also evaluated with Photoshop software in 1 : 1 display. By counting horizontal and vertical distance between the spheres in millimeters on the millimeter-scaled paper the actual 'true' inclination of $\overline{M_1M_2}$ relative to the receptor was calculated by the equation:

$$\gamma = \arctan \frac{\text{horizontal distance [mm]}}{\text{vertical distance [mm]}}.$$

This procedure was also repeated threefold by one observer (RS) and the resulting mean is referred to as 'true inclination'.

Results

Considerable standard deviations (s.d.) within the three replicate assessments were found, with a mean s.d. of

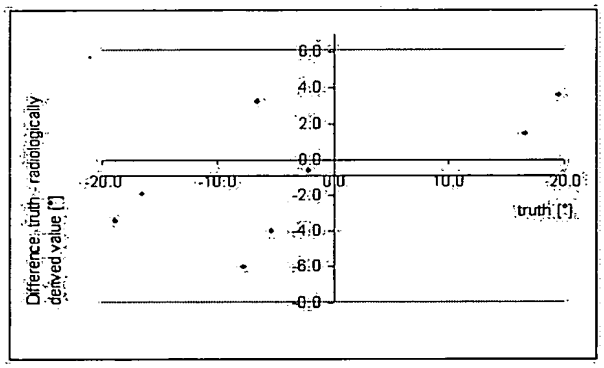

Figure 6 Modified Bland-Altman-plot of observed (true) and calculated values. Differences between truth and calculated angulations (y-axis) are plotted against ground truth on the x-axis, with zero difference indicating maximum accuracy. Limits of tolerance are included in terms of mean difference (dark horizontal line) ± 2 standard deviations (gray shaded horizontal lines). The plot indicates limited accuracy of the method with more over- than under-estimations of the calculated values

2.6°. 'True' and 'calculated' values are compared in Table 2. To obtain information on the actual direction of bias for the calculated differences between truth and radiographically derived values, this calculation is based on absolute values. Otherwise we would have calculated only the magnitude of error, but not its direction with respect to over- or underestimation. Although on average calculated values differed from truth only by −0.9° (s.d. = 3.5°), this was highly significant ($P = 0.000$) as indicated by the Maloney/Rastogi test.[11] The root mean square of the actual differences was 3.4°, also indicating the lack of accuracy.

Differences between truth and calculated values are graphically presented as modified Bland-Altman plots (Figure 6). Differences between individual pairs are plotted against truth, with zero indicating maximum accuracy. Limits of tolerance (gray-shaded horizontal lines) are included in terms of mean difference (dark horizontal line) ± 2 s.d. No value exceeds these limits, however, considerable deviations of single values from truth (range: −6.0°−3.6°) are obvious from the plot, mainly indicating overestimation of truth.

Based on the differences between absolute values, no significant influence of sphere size on accuracy was computed ($P_{Wilcoxon} = 0.715$).

Discussion

Our investigation deals with calculation of actual degree of angular disparity between object and image receptor from intra-oral radiographs acquired in 'paralleling-technique'. Such disparities are common, since the angle is often difficult to control in a clinical situation. Considerable distortion of the images under examination may result from angular discrepancies.[3]

Our method uses two radio-dense objects with rotational symmetry (metallic spheres), with the inter-spherical axis ($\overline{M_1M_2}$) as defined by the connecting line between the centers of the spheres being the axis under examination. Prerequisites for the applicability of the technique are true perpendicular orientation of the central X-ray relative to the receptor in combination with a known point of incidence (0, 0, 0) and a known focus-receptor distance. In principal, the method is based on measurement of magnification of the spheres, since their shadows are elliptically distorted only in one dimension due to their symmetrical design. From these data the position of the respective sphere within the projection system is calculated, and the positions of both spheres relative to a specified receptor axis determine the actual inclination. Although any desired axis within the receptor plane could apply for the investigation, we selected the axis parallel to the long object axis, since angular discrepancies will most probably occur in this direction. If the two spheres are temporarily fixed in a known position to the object of interest (tooth, dental implant), the actual degree and direction of inclination relative to the receptor plane could be calculated. Our method could be used for postoperative monitoring of peri-implant bone height. It is a well known fact, that exact measurements require strict parallelism between fixture and receptor axis.[12,13] This prerequisite could, however, be of less importance if information on the actual inclination was derived from the radiograph, making *a posteriori* correction possible. If for instance the reference spheres were implemented in a temporary abutment fixed in axial direction to the implant during radiographic exposure, this information could be obtained. A distorted linear distance within such an object, such as the vertical long edge of an implant, could then be corrected for distortion. For pre-implant planning, the spheres could also be placed into pre-surgical stents with $\overline{M_1M_2}$ representing the desired implant direction. From the calculated angulation linear bony dimensions in axial direction of the implant could be more accurately corrected for distortion than with any other reference (single sphere, grid). In periodontal assessments of marginal bone height, the spheres could be attached to the proximal surface of a single tooth aligned with its main axis. Linear bone height measurements in this direction could then also be corrected analogously. In addition, information provided by the method could be used in subtraction radiology to limit the degrees of freedom between subsequent radiographs by definition of the position and angulation of an object.[14] Precise calculation, however, requires information of angulation of the object plane relative to the receptor plane in horizontal and vertical direction, which could be obtained from the method by means of a triangle containing three spheres placed in the object plane. We are currently working on the mathematical algorithm for correction of linear distortion from such angulations.

Our experimental data show, that, in principal it is possible to derive the actual degree of angular disparity from the two-sphere reference system. However, with the applied set-up both accuracy as well as reproducibility are clearly not sufficient for clinical use. The trend of overestimation, however, should be seen in the context of the small sample size (eight exposures) and should therefore not be considered as methodological bias. Obviously, our assessments show low reproducibility as indicated by a mean standard deviation of 2.6° (mean)

Table 2 Photographically derived 'true' and radiographically computed values for all images of both series. Note, that for calculation of the difference between truth and calculated value the signs (directions) of the angles were omitted to obtain information on the direction of the bias

Series/image No.	*True inclination (°)*	*Calculated inclination (°) ± s.d.*	*Truth−calculated value (°)*
IX/2A (r_1)	−16.6	−18.5 ± 1.8	−1.9
IX/2B (r_1)	−7.8	−13.8 ± 2.5	−6.0
IX/2C (r_1)	19.5	15.9 ± 1.3	3.6
IX/2D (r_1)	−6.5	−3.2 ± 3.7	3.3
X/2A (r_2)	−2.2	−2.8 ± 3.7	−0.6
X/2B (r_2)	16.6	15.1 ± 5.5	1.5
X/2C (r_2)	−5.4	−9.4 ± 0.9	−4.0
X/2D (r_2)	−19.0	−22.4 ± 1.5	−3.4

s.d., standard deviation; r, radius of reference spheres (r_1: 5.00 mm; r_2: 3.15 mm)

between single assessments. The design of the experimental set-up is one fundamental origin of error. Presumably, marking of the essentially important point of incidence of the central ray (point zero) with the steel-sphere mounted in the center of the tube aperture was not sufficiently accurate, and in addition, its shadow was blurred due to the long sphere-receptor distance (45.30 mm, Table 1). Technically this problem could be resolved by means of a rigid holding device with a mould for the digital receptor centered relative to the central X-ray in such a way, that the central receptor pixel represents point zero (0,0,0). The device must also ensure a true perpendicular alignment of the central ray relative to the receptor and a normal cone length should be used. The latter is recommended since a long cone would result in less magnification and, consequently, in increasing method error.

Another source of error is the assessment procedure of magnification and shadow location, which was performed by simple linear image measurements. Accuracy of the method is strongly depending on measurements of the dimensional changes ($\overline{R_i'S_i'}$), with an approximate magnitude ranging between 0.01 mm and 0.1 mm, dependent on the actual position of the sphere within the system and on the diameter of the spheres. Digital images are limited with respect to the spatial resolution due to their discrete sampling character. Hence we needed a receptor with a small pixel size and the option to display each pixel separately (1 : 1 mode). The RVG 5 CCD-sensor provides a pixel size of 0.0195 mm^2 and the software incorporates the option to display each pixel without pixel-binning. Consequently, changes exceeding 0.0195 mm can theoretically be detected with this receptor, yielding sufficient resolution for our method. In theory, one would expect better accuracy for reference spheres with larger diameters, since absolute dimensional changes are larger with increasing diameter. For the small sample size, however, no such trend was evident from the data. At the same time, correct detection of those pixels that determine the end-points of the assessed distance is of fundamental importance for the accuracy of the procedure. We encountered two major problems during this procedure. First, the difficulty to select the correct pixel and second, to mark this pixel with the mouse-driven cross-shaped cursor. In addition, on a discrete pixel matrix, distances can only be defined by a multiple of whole pixels, with the result possibly being an odd number. Bisecting of such distances then produces 'half' pixels, which then have to be assigned either to one or the other side of the distance assessed by subjective decision of the reader. Automated image enhancement and registration would facilitate standardization of the assessment problem. Since we have an *a posteriori* situation when calculating parameters based on information derived from a given radiograph, image registration features as described by Lehmann *et al.* apply, with the images of the spheres representing extrinsic features.[15] Automated detection of local contrast (defined as brightness difference between two neighbouring pixels) allows for accurate finding of simple structures as presented by the sphere images. By means of grayscale spreading and a predefined threshold those discs could be accurately detected, followed by an automated assessment of all required distances. In addition, assessment of the area of the shadow instead of the distance $\overline{R_i'S_i'}$ itself and then calculating $\overline{R_i'S_i'}$ from the principal axis of the ellipse could presumably enhance accuracy. These procedures could be implemented in any radiographic imaging software. We are currently initiating a software development for these purposes in our department.

In conclusion, our data show that it is possible to derive information *a posteriori* on the actual inclination between a receptor axis of interest and an object temporarily equipped with two spheres. Refinements to the method may increase the accuracy to a clinically acceptable level and further research is required. Currently, no other method exists providing equal information on this geometrical parameter inducing distortion on radiographic images.

References

1. Hausmann E. Radiographic and digital imaging in periodontal practice. *J Periodontol* 2000; **71:** 497–503.
2. van Aken J. Optimum conditions for intraoral roentgenogramms. *Oral Surg Oral Med Oral Pathol Oral Radiol Endod* 1969; **27:** 475–491.
3. Schulze R, d'Hoedt B. Mathematical analysis of projection errors in "paralleling technique" with respect to implant geometry. *Clin Oral Impl Res* 2001; **12:** 364–371.
4. Webber RL, Ruttimann UE, Groenhuis RAJ. Computer Correction of projective Distortions in Dental Radiographs. *J Dent Res* 1984; **63:** 1032–1036.
5. Dubrez B, Jacot-Descombes S, Cimasoni G. Reliability of a paralleling instrument for dental radiographs. *Oral Surg Oral Med Oral Pathol Oral Radiol Endod* 1995; **80:** 358–364.
6. Zappa U, Simona C, van Aken J. In vivo determination of radiographic projection errors produced by a novel filmholder and an X-ray beam manipulator. *J Periodontol* 1991; **62:** 674–683.
7. Eickholz P, Dörfer C, Staehle HJ. Reproduzierbarkeit standardisierter Bissflügelaufnahmen bei Patienten mit fortgeschrittener Parodontitis. *Dtsch Zahnärztl Z* 1994; **49:** 398–402.
8. Webber RL, Horton RA, Tyndall DA, Ludlow JB. Tuned-aperture computed tomography (TACT). Theory and application for three-dimensional dento-alveolar imaging. *Dentomaxillofac Radiol* 1997; **26:** 53–62.
9. Robinson SB, Hemler PF, Webber RL. A geometric problem in medical imaging. *Proc SPIE* 2001; **4121:** 208–217.
10. Webber RL, Bettermann W. A method for correcting errors produced by variable magnification in three-dimensional tuned-aperture computed tomography. *Dentomaxillofac Radiol* 1999; **28:** 305–310.
11. Krummenauer F, Doll G. Statistical methods for the comparison of measurements derived from orthodontic imaging. *Eur J Orthod* 2000; **22:** 257–269.
12. Sewerin IP. Errors in radiographic assessment of marginal bone height around osseointegrated implants. *Scand J Dent Res* 1990; **98:** 428–433.
13. Payne AGT, Solomons YF, Lownie JF. Standardization of radiographs for mandibular implant-supported overdentures: review and innovation. *Clin Oral Impl Res* 1999; **10:** 307–319.
14. Lehmann TM, Gröndahl K, Gröndahl H-G, Schmitt W, Spitzer K. Observer-independent registration of perspective projection prior to substraction of *in vitro* radiographs. *Dentomaxillofac Radiol* 1998; **27:** 140–150.
15. Lehmann TM, Gröndahl H-G, Benn DK. Computer-based registration for digital subtraction in dental radiology. *Dentomaxillofac Radiol* 2000; **29:** 323–346.

#2

Determination of projection geometry from quantitative assessment of the distortion of spherical references in single-view projection radiography

Ralf Schulze,[a] Dan Dominik Bruellmann, Felix Roeder, and Bernd d'Hoedt
Department of Oral Surgery (and Oral Radiology), Johannes Gutenberg-University, Dental School, Augustusplatz 2, Mainz, 55131 Germany

(Received 24 June 2003; revised 11 June 2004; accepted for publication 30 July 2004; published 28 September 2004)

A method is introduced, inferring the three-dimensional (3-D) location from the 2-D radiographic shadow of an opaque spherical reference body of known radius by considering its elliptical distortion, the 2-D shadow location and a known source-to-receptor distance. Three noncollinear spheres fixed to a rigid object constitute all possible degrees of freedom, i.e., the entire 3-D imaging geometry. The method may be used (a) to determine the 3-D imaging geometry from a single 2-D view and (b) to correct for foreshortening of object distances coplanar with the plane defined by the sphere triplet. Apart from the mathematical background the article describes a small feasibility experiment, performed with four different sphere diameters and a commercial dental ccd-receptor system (pixel length: 0.0195 mm). The mouse-cursor based image evaluation revealed an average underestimation of the critical depth- (x-) coordinate decreasing with increasing radius (−30.3% for r=0.5 mm to 2.8% for r=2.5 mm). Intraobserver reliability (the standard deviation between three single cursor-based assessments) ranged between 0% and 8% of the actual true depth. The main source of the input error is associated with the assessment of the amount of elliptical distortion, where subpixel accuracy is demanded. Consequently, software-based automated image evaluation is required using available methods for pattern recognition and point-spread correction. Provided sufficient accuracy, the method provides an important tool for foreshortening correction, depth assessment, motion analysis, and 3-D reconstruction from two or more 2-D views. © *2004 American Association of Physicists in Medicine.* [DOI: 10.1118/1.1796951]

I. INTRODUCTION

The spatial relation between x-ray source, object, and imaging plane relative to one another during exposition, i.e., the projection or imaging geometry, fundamentally determines the two-dimensional (2-D) radiographic image formation. Since three-dimensional (3-D) reconstruction is commonly based on the determination of the imaging geometry,[1–6] its knowledge enables straightforward 3-D reconstruction from at least two 2-D images obtained under different geometries.[7,8] Knowing the imaging geometry is also helpful to calculate the magnification and foreshortening of objects appearing in the image. Such effects are very common, particularly in dental intra-oral radiography, where anatomical barriers (e.g., the hard palate) preclude a parallel positioning of object and image plane. Commonly, spherical reference markers are used for calibration,[9–12] preferably in combination with a holding device[13–15] coupling the receptor to the source in a c-arm fashion. In medical radiography, metallic reference markers[16,17] or other objects of known dimensions, e.g., angiographic catheters,[18,19] are used as calibration objects. Despite their frequent use in dental[9–12] as well as medical[20,21] radiography or for tomosynthetic reconstruction,[4,5] so far only magnification[9–12,20,21] or the 2-D shadow position[4,5] of spherical reference bodies was considered, thereby neglecting the depth information inherent in the elliptical distortion. Depth information, however, is essential for the calculation of the imaging geometry. Hoffmann *et al.* introduced a method to determine the 3-D position of a general sparse object from a single view by using *a priori* knowledge of relative marker positions.[22] Reference spheres have already been used for 2-D assessment of the angular relationship between an object and a given receptor axis.[23] We aim at the extension of this method to the third dimension to obtain their 3-D position from a single projection. It will shown that from quantitative exploitation of the 2-D shadows of three noncollinear reference spheres fixed to an object under study, the imaging geometry of the exposure can be determined, if the source-to-receptor distance is known. A particular application of this method for the foreshortening and magnification correction of objects coplanar with the reference plane determined by the sphere triplet will also be addressed. In addition, results of a small feasibility experiment are presented.

II. METHODS

A. Mathematical model

1. Calculation of the 3-D reference sphere coordinates

Consider a cone-beam projection in a Cartesian coordinate system (Fig. 1), where the central x ray (aligned with the x axis), i.e., the orthogonal shortest distance between a spot source $F(x_F,0,0)$ and a flat $y-z$-receptor plane incides the latter in the origin $O'(0,0,0)$. Let all 2-D images points be denoted by an apostrophe. The points of incidence of the diverging beam may be considered as an infinite number of concentric circles with center point $O'(0,0,0)$. Thus, the maximum magnification on the 2-D image plane will occur

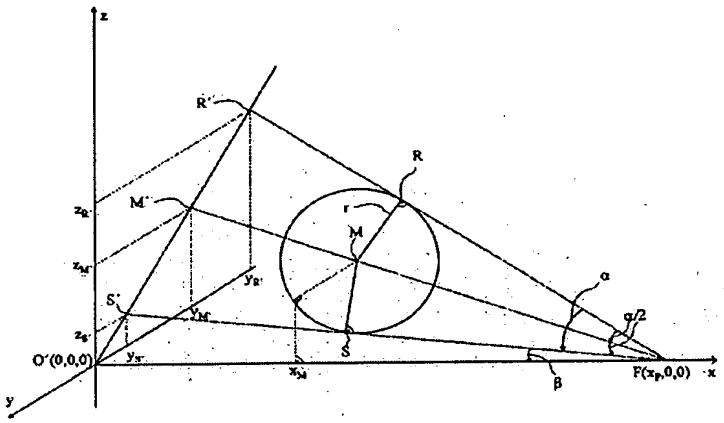

FIG. 1. Exposed from a focal spot $F(x_F,0,0)$, the maximum magnification defining the major ellipse axis $\overline{R'S'}$ occurs along a line through the point of incidence $O'(0,0,0)$ of the central x ray on the flat y–z–image plane. $R'(0,y_{R'},z_{R'})$ and $S'(0,y_{S'},z_{S'})$ represent the 2-D images of the 3-D sphere tangent points $R(x_R,y_R,z_R)$ and $S(x_S,y_S,z_S)$. They subtend an angle α between $R'F S'$; β denotes the angle $S' F O'$. Note, that the image $M'(0,y_{M'},z_{M'})$ of the desired 3-D sphere center point $M(x_M,y_M,z_M)$ does not coincide with the ellipse center, i.e., does not bisect the long ellipse axis $\overline{R'S'}$.

along vectors pointing from O' toward the periphery. We aim for the localization of a given sphere (radius: r), i.e., its center of mass point $M(x_M,y_M,z_M)$ from its shadow that will be an ellipse (for proof see Ref. 24), except for an orthogonal projection, where it will form a circular disk. The projection lines tangent to the 3-D sphere tangent points $R(x_R,y_R,z_R)$ and $S(x_S,y_S,z_S)$ cast the major ellipse axis $\overline{R'S'}$, the extension of which will necessarily intersect with O' due to the direction of 2-D magnification. The angle α (Fig. 1) between $R'F$ and S' is given by

$$\alpha = \tan^{-1}\frac{\overline{O'R'}}{x_F} - \beta, \tag{1}$$

where

$$\beta = \tan^{-1}\frac{\overline{O'S'}}{x_F}. \tag{2}$$

Please note that the image M' of the sphere's center point M does not coincide with the center of the ellipse cast by the sphere. The distance between M and the spot source F is obtained from

$$|\overline{FM}| = \frac{r}{\sin\frac{\alpha}{2}}. \tag{3}$$

From the theorem of intersecting lines we obtain the desired 3-D coordinates of M from

$$x_M = x_F - |\overline{FM}|\cos\left(\frac{\alpha}{2}+\beta\right), \tag{4}$$

$$y_M = \frac{y_{M'}|\overline{FM}|\cos\left(\frac{\alpha}{2}+\beta\right)}{x_F}, \tag{5}$$

$$z_M = \frac{z_{M'}|\overline{FM}|\cos\left(\frac{\alpha}{2}+\beta\right)}{x_F}. \tag{6}$$

The 3-D coordinates of the center points M_1, M_2, M_3 of the three noncollinear spheres temporarily to a rigid object under study provides the 3-D locations of three "object" points. $0'(0,0,0)$ may simply be reconstructed from intersecting the lines extended through the long elliptical axes, or, in the presence of error, from the point of closest approach between these lines. Together with the known source-to-receptor distance x_F, this information constitutes the spatial relation between the source and image receptor, leaving the object three translational and three rotational degrees of freedom. These are sufficiently constituted by the three points in space (M_1,M_2,M_3) obtained from Eqs. (4)–(6).[25]

2. Correction of foreshortening for within-reference-plane objects

If the noncollinear sphere triplet is placed coplanar with an object Q or a distance under examination (Fig. 2), the plane P defined by M_1, M_2, M_3:

$$A_1x + A_2y + A_3z + A = 0, \tag{7}$$

with A_i obtained from the determinant

$$\begin{vmatrix} x-x_1 & y-y_1 & z-z_1 \\ x_2-x_1 & y_2-y_1 & z_2-z_1 \\ x_3-x_1 & y_3-y_1 & z_3-z_1 \end{vmatrix} = 0, \tag{8}$$

may be rotated about the y axis at an arbitrary angle γ and about the z axis an angle ϵ, respectively. By backprojecting a given point $T'(x_{T'},y_{T'},z_{T'}) \in Q'$ onto P, we find its actual 3-D position $T(x_T,y_T,z_T) \in Q$ from intersecting the line through $\overline{FT}$ with P. The equation of a line-plane intersection[26] yields (for a derivation see the Appendix):

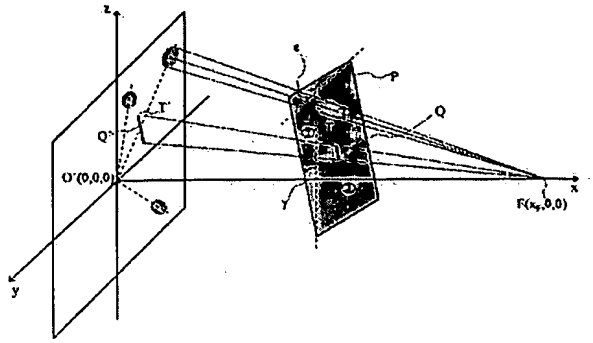

FIG. 2. If the sphere-triplet is placed coplanar with an object Q under examination, any object image point $T'(x_{T'},y_{T'},z_{T'}) \in Q'$ can be back-projected onto the reference plane P, yielding its true 3-D position $T(x_T,y_T,z_T) \in Q$.

$$x_T = -\frac{A_2 y_{T'} + A_3 z_{T'} + A}{A_1 + A_2\left(-\frac{y_{T'}}{x_F}\right) + A_3\left(-\frac{z_{T'}}{x_F}\right)}. \tag{9}$$

The remaining coordinates are given by

$$y_T = x_T\left(-\frac{y_{T'}}{x_F}\right) + y_{T'}, \tag{10}$$

and

$$z_T = x_T\left(-\frac{z_{T'}}{x_F}\right) + z_{T'}. \tag{11}$$

B. Experimental evaluation

Four acrylic phantoms (thickness: 2.0 mm), each containing three isometric steel spheres (0.5, 1.0, 1.5, and 2.5 mm) and two pieces of steel-wire "objects" (diameter: 0.6 mm; lengths: 8.90 or 16.20 mm) with needle-shaped ends, were exposed separately on an optical bench with a fabrication accuracy of 0.1 to 0.2 mm. The point of incidence $O'(0,0,0)$ of the central x ray coincided with the center of a dental ccd receptor (Full Size, Sirona Dental Systems GmbH, Bensheim, Germany; physical pixel size: 0.0195 mm $\times$ 0.0195 mm) to within ± 10 pixels. This design eliminated additional errors to be expected from distortion-based origin reconstruction from only minimally distorted shadows on the small-size (26 mm $\times$ 34 mm) sensor area. Since no image intensifier or fiber-optic taper was used and the sensor size was very small, negligible pincushion distortion is assumed. Each phantom was exposed at three time settings (0.06, 0.08, and 0.10 s) and eight different angulations (range: $-57.7°$ to $-46.7°$) relative to the image receptor, occurring about the y axis and the z axis (Fig. 2). Within the series of 0.08 s exposure time, scatter equivalents of one, three, or five wax plates (thickness: 1.5 mm) were employed in a stepwise fashion. Due to the construction of the optical bench, x_F ranged between 254.3 and 294.1 mm. For the mouse-driven manual image evaluation process, the eight bit uncompressed tiff files were imported into an image editing software (Photoshop 7.0, Adobe Software Inc., Mountain View, California).

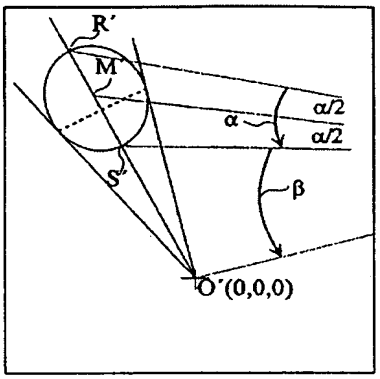

FIG. 3. Using the mouse-driven cursor, tangents were manually drawn from the origin O' to both sides of the elliptical sphere shadow. The distance between the tangent points was bisected and the resulting point connected to O'. The inner (S') and outer (R') endpoint of major elliptical axis is found by intersecting this line with the ellipse boundary. The image M' of the 3-D sphere's center point M and the out of plane angles α and β with their respective connecting lines to the focal spot F are included here only to illustrate the spatial relationships.

$O'(0,0,0)$ was defined as one of the four central pixels on the even pixel matrix. Without windowing or leveling of the image, tangents were constructed from O' to each ellipse from both sides, and the resulting tangent point connection line was bisected (Fig. 3). By extending the line through this bisection point and O' through the elliptical shadow, the inner (S') and outer (R') point of intersection with the ellipse boundary was identified and their pixel coordinates recorded. The coordinates of the steel-wire object endpoints as assessed along their long axis were also recorded. After conversion into millimeters, the data were fed into the algorithm implemented in a spread sheet software (Microsoft Excel 2000, Microsoft Corporation, Redmond, CA). True coordinates of the sphere centers (M_1, M_2, M_3) were assessed to the nearest 0.5 mm with a caliper. As this error propagates into our calculated depth (x) errors on a one-to-one basis, our experimental data include an intrinsic measurement error of ± 0.5 mm. Differences between calculated and true values were defined as absolute depth errors, δx. The relative depth errors were computed from $\delta x/x$. Intraobserver variability (reproducibility) of the manual landmark identification and marking process was calculated from the standard deviation between three assessments on one arbitrarily selected image of each sphere radius, separated by a time interval of three days.

III. RESULTS

The mean relative error in the depth averaged over all images obtained with one reference radius was largest (-30.3%) for $r = 0.5$ mm. For all other diameters, it ranged

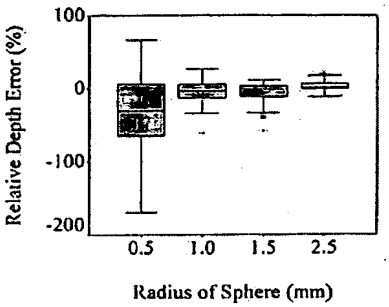

FIG. 4. Experimental relative depth errors presented in box plots, where each box defines the interquartile distance (IQR) between the 25% and 75% quartile (median: bold horizontal line). T-shaped whiskers mark all values (outliers) lying ≤1.5 IQR beyond the quartiles; extreme values exceeding these limits are indicated by asterisks. The plots illustrate a trend of the underestimation of truth decreasing together with the box heights with a larger sphere radius.

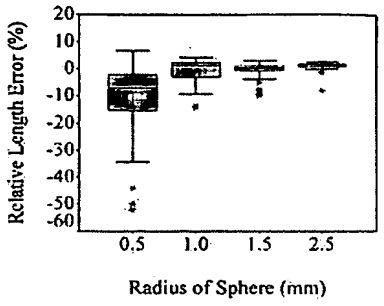

FIG. 6. Box plots (for details see Fig. 4) of length assessment accuracy, which clearly increased with the sphere radius.

between −6.5%(r=1.5 mm) and 2.8% (r=2.5 mm). The 95% Confidence Intervals (95% CI) were continuously decreasing with increasing reference sphere radius. The results show a clear underestimation of depth, i.e., most of the x coordinates were short of the truth (Table I; Fig. 4). Accuracy in x coordinates was clearly correlated with the amount of scatter equivalent (Spearman Rho =0.490, $r<0.001$; Fig. 5), with the absolute errors increasing with the latter. The mean error in object length was largest (11.3%) for the smallest reference sphere radius (r=0.5 mm), and relatively similar (±1%) for all remaining diameters. The 95% CI's of this error followed the same pattern as for the x coordinates (Table I; Fig. 6). The standard deviation between single assessments (reproducibility) performed by one observer (F.R.) ranged between 0% and 8% of the true depth value.

IV. DISCUSSION

The algorithm infers the 3-D locations of spherical reference bodies from their elliptically distorted shadows. Spheres are frequently used in radiology,[4,9–11,20,27–33] e.g., in radiostereometry (RSA);[29–33] 3-D reconstruction from 2-D views,[4,5,34] or local magnification assessment in dental intra-oral,[10,11,27,28] panoramic,[9] or cephalometric[34] radiography. All these techniques, however, only consider magnification[9–11,20,21,27,28] or the 2-D position[4,5,28–34] of the marker image, yet not its elliptical distortion. This geometric information together with the knowledge of one distance in space (the source-to-receptor distance), however, is sufficient to compute the sphere's center point's 3-D coordinates within the projection geometry from a single projection. Unlike the method described by Hoffmann and Esthappan,[22] the algorithm computes the correspondence between object and image points from large image features (the sphere shadows) by means of geometric *a priori* knowledge. Hence, the identification of image landmark points should be substantially easier than in other methods.[3,4,6,22] Three noncollinear spheres attached to the object under study provide three known "object" points in space, thereby constituting its possible six degrees of freedom.[25] If not known *a priori*, the point of incidence of the central x ray on the receptor plane may be reconstructed from the point of closest approach between the extended lines through at least two major elliptical shadow axes. Interestingly, another device especially constructed for an accurate location of the point of the central x-ray incidence is also based on the divergent projection vectors on a flat image plane.[35] Once the imaging geometry is known, the 3-D reconstruction of the information inherent in at least two 2-D views obtained under different geometries is a straightforward task.[5,6] Hence, the algorithm may be used for image registration prior to the reconstruction process.

If an object (distance) is coplanar with the sphere triplet, its true dimensions may be obtained from simple backprojection. This may be used, if the spatial orientation of the desired dimension within the human body can be roughly estimated *a priori*. In this case, Eqs. (9)–(11) provide the true 3-D coordinates of any point identifiable in the image. A possible extension would be to attach several reference spheres roughly following the object shape, allowing for the formation of multiple triplets coplanar to specific parts of the object. This would make sense for the evaluation of larger structures (for instance, skull or chest radiographs), where more than one internal structure is under examination.[36]

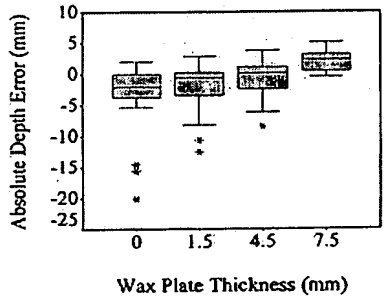

FIG. 5. Box plots (for details see Fig. 4) of experimental absolute depth errors within the set of 0.8 s exposure time plotted against the scatter equivalent thickness. Except for the maximum wax plate thickness (7.5 mm), again a trend of the underestimation of truth is evident.

TABLE I. The relative error in the calculated reference sphere depth (x) coordinates and resulting errors in the calculated object length for the four reference sphere radii. Bold values highlight the smallest errors in the respective row. CI: Confidence Interval.

Sphere radius (mm)	0.5	1.0	1.5	2.5
X-coordinate % error				
Mean value	−30.3	−4.9	−6.5	**2.8**
95%-CI	−139.4–78.8	−35.7–25.9	−34.2–21.2	−11.6–17.2
Object-length % error				
Mean value	11.3	0.6	0.4	−1.0
95%-CI	−16.7–39.3	−8.1–9.3	−5.4–6.2	−4.5–2.5

Operational problems include occlusion by the sphere shadows, particularly in small area dental radiographs, and difficulties in attaching the spheres to small-size objects such as teeth. However, the latter has been demonstrated *in vivo* elsewhere[12,37] Apart from geometric unsharpness and other sources of noise, geometric errors will affect the method's accuracy in locating the spheres in three dimensions (for a detailed analysis see the internet EPAPS version of this document). Small errors in x_F and in the location of O' will have a negligible influence. However, an accurate identification of the image points R' and S' is crucial, since they determine the angle α between the tangent projection lines, into which the algorithm fits the known sphere size. The simplified case of an orthogonal projection ($\beta=0$), where $x_M=x_F-\overline{FM}$ and Eq. (4) yields $x_M=x_F-r/\sin(\alpha/2)$, also clearly illustrates the influence of the sphere radius r. One pixel error propagates into a depth error ranging between 14%(r=2.0 mm) and 40%(r=0.5 mm) for a typical dental configuration (x_F =200 mm; pixel size: 0.039 mm) vs 32%(r=5.0 mm) to 75%(r=2.0 mm) for a typical medical radiographic situation (x_F=1000 mm; pixel size: 0.130 mm). A small pixel size, i.e., a high resolution, reduces errors caused by the discrete image nature. Subpixel accuracy in the assessment of the critical major elliptical axis dimension should be aimed for. The experiment only performed to prove the principle feasibility of the method yielded depth coordinates short of truth, i.e., an underestimation of the major ellipse axis $|\overline{R'S'}|$ most probably due to low local contrast at the shadow's boundary. Despite an expected size overestimation for small objects due to the well-known point spread effect,[38] pixels were obviously incorrectly manually assigned to background, although in fact belonging to $\overline{R'S'}$.

Future work will focus on a software implementation of the algorithm to enhance accuracy. Possible solutions include a generalized Hough Transform[39] for automated sphere shadow detection in combination with a subpixel fitting procedure similar to that described in Ref. 32. Geometric unsharpness could be addressed by deconvolution with a mathematically modeled inverse point spread function. Also, the ellipse main axis dimension could be corrected by weighting of the gray values' first and second derivative along the scan line $\overline{R'S'}$.[38] Once an acceptable limit of accuracy is achieved, our research will be directed toward 3-D reconstruction from 2-D views. For this purpose, the method will be used for simplified registration of the 2-D images in a modified Metz–Fencil technique.[3]

ACKNOWLEDGMENTS

This work, including parts of the thesis of Felix Roeder entitled "Generalization, theoretical and experimental evaluation of an algorithm determining the imaging geometry from quantitative analysis of the radiographic shadows of spherical reference bodies," was supported by the German Research Foundation (Deutsche Forschungsgemeinschaft DFG, Grant No. SCHU 1496/1-1).

APPENDIX: DERIVATION OF EQ. (9)

From the general equation of a plane in three dimensions [Eq. (7)] and the line intercept form equations:

$$y = kx + a \tag{A1}$$

and

$$z = hx + b, \tag{A2}$$

we obtain the x coordinate of the point of intersection $T(x_T,y_T,z_T)$ between the plane and the line by substituting y and z from (A1) and (A2) in Eq. (7) and solving for x:

$$x_T = -\frac{A_2a + A_3b + A}{A_1 + A_2k + A_3h}. \tag{A3}$$

Setting x=0, Eqs. (A2) and (A3) yield $y=a$ and $z=b$. Inserting the parameters h and k in Eq. (A3) as obtained from Eqs. (10) and (11), yields the final form of Eq. (9):

$$x_T = -\frac{A_2y_{T'} + A_3z_{T'} + A}{A_1 + A_2\left(-\frac{y_{T'}}{x_F}\right) + A_3\left(-\frac{z_{T'}}{x_F}\right)}. \tag{A4}$$

a)Electronic mail: rschulze@mail.uni-mainz.de

[1]H. C. Kim, B. G. Min, T. S. Lee, S. -J. Lee, C. W. Lee, J. H. Park, and M. C. Han, "Three-dimensional digital subtraction angiography," IEEE Trans. Med. Imaging **1**, 152–158 (1982).
[2]K. R. Hoffmann, C. E. Metz, and Y. J. Chen, "Determination of 3D imaging geometry and object configurations from two biplane views: An

enhancement of the Metz–Fencil technique," Med. Phys. 22, 1219–1227 (1995).
[3]C. E. Metz and L. E. Fencil, "Determination of three-dimensional structure in biplane radiography without prior knowledge of the relationship between the two views: Theory," Med. Phys. 16, 45–51 (1989).
[4]R. L. Webber, R. A. Horton, D. A. Tyndall, and J. B. Ludlow, "Tuned-aperture computed tomography (TACT). Theory and application for three-dimensional dento-alveolar imaging," Dentomaxillofac Radiol. 26, 53–62 (1997).
[5]S.-Y. J. Chen and J. D. Caroll, "3-D reconstruction of coronary arterial tree to optimize angiographic visualization," IEEE Trans. Med. Imaging 19, 318–336 (2000).
[6]H. C. Longuet-Higgins, "A computer algorithm for reconstructing a scene from two projections," Nature (London) 293, 133–135 (1981).
[7]S. B. Robinson, P. F. Hemler, and R. L. Webber, "A geometric problem in medical imaging," Proc. SPIE 4121, 208–217 (2000).
[8]F. Cheriet and J. Meunier, "Self-calibration of a biplane X-ray imaging system for an optimal three dimensional reconstruction," Comput. Med. Imaging Graph. 23, 133–141 (1999).
[9]N. Behneke and P. Tetsch, "Diagnostik und Planung von Implantaten im zahnlosen Unterkiefer," Fortschr. Zahnaerztl. Implantol. 1, 266–271 (1985).
[10]E. H. Verdonschot, A. J. Sanders, and A. J. Plasschaert, "A computer-aided image analysis system for area measurement of tooth root surfaces," J. Periodontol. 61, 275–280 (1990).
[11]E. H. Verdonschot, A. J. Sanders, and A. J. Plasschaert, "Applicability of an image analysis system in alveolar bone loss measurement," J. Clin. Periodontol. 18, 30–36 (1991).
[12]M. S. Reddy and I.-C. Wang, "Radiographic determinants of implant performance," Adv. Dent. Res. 13, 136–145 (1999).
[13]E. Hausmann, "Radiographic and digital imaging in periodontal practice," J. Periodontol. 71, 497–503 (2000).
[14]A. G. T. Payne, Y. F. Solomons, and J. F. Lownie, "Standardization of radiographs for mandibular implant-supported overdentures: Review and innovation," Clin. Oral Implants Res. 10, 307–319 (1999).
[15]R. Schulze and B. d'Hoedt, "Mathematical analysis of projection errors in 'paralleling technique' with respect to implant geometry," Clin. Oral Implants Res. 12, 364–371 (2001).
[16]J. A. Horton, "Sizing rings: A simple technique for measuring intracranial lesions," AJNR Am. J. Neuroradiol. 16, 1449–1451 (1995).
[17]Z. Wang, S. Rudin, D. R. Bednarek, and L. Miskolczi, "Improved method of magnification factor calculation for the angiographic measurement of neurovascular lesion dimensions," J. Appl. Clin. Med. Phys. 3, 255–259 (2002).
[18]J. H. C. Reiber, C. J. Kooijman, C. J. Slager, J. J. Gebrans, J. C. H. Schuurbiers, A. Den Boer, W. Wijns, P. W. Serrus, and P. G. Hugenholtz, "Coronary artery dimensions from cineangriograms—Methodology and validation of a computer assisted analysis procedure," IEEE Trans. Med. Imaging 3, 131–141 (1984).
[19]J. H. C. Reiber, W. Jukema, A. van Boven, R. M. van Houdt, K. I. Lie, and A. V. G. Bruschke, "Catheter sizes for quantitative coronary arteriography," Cathet Cardiovasc. Diagn. 33, 153–155 (1994).
[20]K. Burckhardt, Ch. Gerber, J. Hodler, H. Noetzli, and G. Szekely, "Precision of distance determination using 3D to 2D projections: The error of migration measurement using X-ray images," Med. Image Anal 4, 375–388 (2000).
[21]C. Wiedenhoefer, F. S. Glander, S. L. Gage, and P. Katsch, "Radiographic reference marker," U.S. Patent 6,459,772, 2002.
[22]K. R. Hoffmann and J. Esthappan, "Determination of three-dimensional positions of known sparse objects from a single projection," Med. Phys. 24, 555–564 (1997).
[23]R. Schulze and B. d'Hoedt, "A method to calculate angular disparities between object and receptor in 'paralleling technique'," Dentomaxillofac Radiol. 31, 32–38 (2002).
[24]D. Hilbert and S. Cohn-Vossem, "The cylinder, the cone, the conic sections and their surfaces of revolution," in *Geometry and Imagination*, reprint ed. (Chelsea Publishing, New York, 1999), pp. 7–9.
[25]M. Betke, H. Hong, D. Thomas, C. Prince, and J. P. Ko, "Landmark detection in the chest and registration of lung surfaces with an application to nodule registration," Med. Image Anal 7, 265–281 (2003).
[26]L. N. Bronstein, K. A. Semendjajew, G. Musiol, and H. Muehlig, *Taschenbuch der Mathematik*, 2nd ed. (Verlag Harri Deutsch, Frankfurt am Main, 1995).
[27]J. Handschel, J. Kleinheinz, M. Kelker, I. Reuter, and U. Joos, "Reproducible X-ray projection geometry in endentulous patients," Dentomaxillofac Radiol. 28, 368–371 (1999).
[28]M. K. Nair, A. Seyedain, S. Agarwal, R. L. Webber, U. P. Nair, N. P. Piesco, M. P. Mooney, and H. G. Groendahl, "Tuned aperture computed tomography to evaluate osseous healing," J. Dent. Res. 80, 1621–1624 (2001).
[29]N. Boerlin, "Comparison of resection-intersection algorithms and projection geometries in radiostereometry," Photogrammetria (ISPRS) 56, 390–400 (2002).
[30]N. Boerlin, T. Thien, and J. Kaerrholm, "The precision of radiostereometric measurements: Manual vs. digital measurements," J. Biomech. 35, 69–79 (2002).
[31]E. R. Valstar, H. A. Vrooman, S. Tokksvig-Larsen, L. Ryd, and R. G. H. H. Nelissen, "Digital automated RSA compared to manually operated RSA," J. Biomech. 33, 1593–1599 (2000).
[32]H. A. Vrooman, E. R. Valstar, G.-J. Brand, D. F. Admiraal, P. M. Rozing, and H. C. Reiber, "Fast and automated measurements in digitized stereophotogrammetric radiographs," J. Biomech. 31, 491–498 (1998).
[33]X. Yuan and L. Ryd, "Accuracy analysis for RAS: A computer simulation study on 3D marker reconstruction," J. Biomech. 33, 493–498 (2000).
[34]M. M. Rousset, F. Simonek, and J. P. Dubus, "A method for correction of radiographic errors in serial three-dimensional cephalometry," Dentomaxillofac Radiol. 32, 50–59 (2003).
[35]D. K. Freeman, "Testing coincidence of x-ray and light beam," Med. Phys. 11, 78 (1984).
[36]F. H. Fahey, L. K. Rhyasen, B. A. Harkness, M. A. Meltsner, and R. L. Webber, "Angular disparity in ETACT scintimammography," Med. Phys. 29, 1980–1983 (2002).
[37]R. L. Webber and J. K. Messura, "An *in vivo* comparison of diagnostic information obtained from tuned-aperture computed tomography and conventional dental radiographic imaging modalities," Oral Surg. Oral Med. Oral Pathol. Oral Radiol. Endod. 88, 239–247 (1999).
[38]J. Beier, H. Oswald, U. Sauer, and E. Fleck, "Accuracy of measurement in quantitative coronary angiography (QCA)," in *Computer Assisted Radiology (CAR 91)*, edited by H. U. Lemke, M. L. Rhodes, C. C. Jaffe, and R. Felix (Springer-Verlag, Berlin, 1991), pp. 721–726.
[39]D. H. Ballard, "Generalizing the Hough transform to detect arbitrary shapes," Pattern Recogn. 13, 111–122 (1981).